Calhoun: The NPS Institutional Archive

DSpace Repository

Theses and Dissertations | 1. Thesis and Dissertation Collection, all items

2022-06

RESOLUTION DEPENDENCE OF ACOUSTIC SCATTERING STATISTICS FOR COMPLEX SEAFLOORS

Lehman, Alexander J.

Monterey, CA; Naval Postgraduate School

https://hdl.handle.net/10945/70737

This publication is a work of the U.S. Government as defined in Title 17, United States Code, Section 101. Copyright protection is not available for this work in the United States.

Downloaded from NPS Archive: Calhoun

http://www.nps.edu/library

Calhoun is the Naval Postgraduate School's public access digital repository for research materials and institutional publications created by the NPS community. Calhoun is named for Professor of Mathematics Guy K. Calhoun, NPS's first appointed -- and published -- scholarly author.

Dudley Knox Library / Naval Postgraduate School
411 Dyer Road / 1 University Circle
Monterey, California USA 93943

NAVAL POSTGRADUATE SCHOOL

MONTEREY, CALIFORNIA

THESIS

RESOLUTION DEPENDENCE OF ACOUSTIC SCATTERING STATISTICS FOR COMPLEX SEAFLOORS

by

Alexander J. Lehman

June 2022

Thesis Advisor: Derek Olson
Second Reader: Mara S. Orescanin

Approved for public release. Distribution is unlimited.

THIS PAGE INTENTIONALLY LEFT BLANK

REPORT DOCUMENTATION PAGE			*Form Approved OMB No. 0704-0188*

Public reporting burden for this collection of information is estimated to average 1 hour per response, including the time for reviewing instruction, searching existing data sources, gathering and maintaining the data needed, and completing and reviewing the collection of information. Send comments regarding this burden estimate or any other aspect of this collection of information, including suggestions for reducing this burden, to Washington headquarters Services, Directorate for Information Operations and Reports, 1215 Jefferson Davis Highway, Suite 1204, Arlington, VA 22202-4302, and to the Office of Management and Budget, Paperwork Reduction Project (0704-0188) Washington, DC 20503.

1. AGENCY USE ONLY *(Leave blank)*	**2. REPORT DATE** June 2022	**3. REPORT TYPE AND DATES COVERED** Master's thesis

4. TITLE AND SUBTITLE RESOLUTION DEPENDENCE OF ACOUSTIC SCATTERING STATISTICS FOR COMPLEX SEAFLOORS	**5. FUNDING NUMBERS** RQQ89
6. AUTHOR(S) Alexander J. Lehman	

7. PERFORMING ORGANIZATION NAME(S) AND ADDRESS(ES) Naval Postgraduate School Monterey, CA 93943-5000	**8. PERFORMING ORGANIZATION REPORT NUMBER**
9. SPONSORING / MONITORING AGENCY NAME(S) AND ADDRESS(ES) Office of Naval Research, Arlington, VA, 22217	**10. SPONSORING / MONITORING AGENCY REPORT NUMBER**

11. SUPPLEMENTARY NOTES The views expressed in this thesis are those of the author and do not reflect the official policy or position of the Department of Defense or the U.S. Government.

12a. DISTRIBUTION / AVAILABILITY STATEMENT Approved for public release. Distribution is unlimited.	**12b. DISTRIBUTION CODE** A

13. ABSTRACT (maximum 200 words)

Unmanned underwater vehicles (UUVs) utilize sonar perception to conduct sea floor mapping and target detection operations. However, systems with different resolutions may generate different probability density functions (PDFs) of the magnitude of the complex pressure. An area of research that has not been adequately studied is the effects of resolution manipulation during the post-processing of high-resolution data from complex seafloor environments. This work analyzed synthetic aperture sonar (SAS) data collected from multiple seafloor geomorphologies surrounding Bergen, Norway, to study the resolution dependence of scattering statistics for complex seafloors. Multi-look methods were applied to reduce the resolution. The original data and reduced resolution data were compared in terms of PDF amplitude and evaluated by standard goodness of fit tests with heavy-tailed statistical models that are commonly used in the radar and sonar community, including mixture models. Top-performing physics-based distributions were analyzed by how well they model how background and clutter parameters change with resolution manipulation. Empirical equations and a table of environmental constants were developed to allow a user to understand better how sonar data behaves at a given resolution and bottom type.

14. SUBJECT TERMS synthetic aperture sonar, sonar, multi-look, scattering statistics	**15. NUMBER OF PAGES** 69
	16. PRICE CODE

17. SECURITY CLASSIFICATION OF REPORT Unclassified	**18. SECURITY CLASSIFICATION OF THIS PAGE** Unclassified	**19. SECURITY CLASSIFICATION OF ABSTRACT** Unclassified	**20. LIMITATION OF ABSTRACT** UU

NSN 7540-01-280-5500

Standard Form 298 (Rev. 2-89)
Prescribed by ANSI Std. 239-18

THIS PAGE INTENTIONALLY LEFT BLANK

Approved for public release. Distribution is unlimited.

RESOLUTION DEPENDENCE OF ACOUSTIC SCATTERING STATISTICS FOR COMPLEX SEAFLOORS

Alexander J. Lehman
Lieutenant Commander, United States Navy
BS, Villanova University, 2012

Submitted in partial fulfillment of the
requirements for the degree of

MASTER OF SCIENCE IN METEOROLOGY AND PHYSICAL OCEANOGRAPHY

from the

NAVAL POSTGRADUATE SCHOOL
June 2022

Approved by: Derek Olson
Advisor

Mara S. Orescanin
Second Reader

Peter C. Chu
Chair, Department of Oceanography

THIS PAGE INTENTIONALLY LEFT BLANK

ABSTRACT

Unmanned underwater vehicles (UUVs) utilize sonar perception to conduct sea floor mapping and target detection operations. However, systems with different resolutions may generate different probability density functions (PDFs) of the magnitude of the complex pressure. An area of research that has not been adequately studied is the effects of resolution manipulation during the post-processing of high-resolution data from complex seafloor environments. This work analyzed synthetic aperture sonar (SAS) data collected from multiple seafloor geomorphologies surrounding Bergen, Norway, to study the resolution dependence of scattering statistics for complex seafloors. Multi-look methods were applied to reduce the resolution. The original data and reduced resolution data were compared in terms of PDF amplitude and evaluated by standard goodness of fit tests with heavy-tailed statistical models that are commonly used in the radar and sonar community, including mixture models. Top-performing physics-based distributions were analyzed by how well they model how background and clutter parameters change with resolution manipulation. Empirical equations and a table of environmental constants were developed to allow a user to understand better how sonar data behaves at a given resolution and bottom type.

THIS PAGE INTENTIONALLY LEFT BLANK

TABLE OF CONTENTS

I. INTRODUCTION....1

II. PREVIOUS LITERATURE....7

III. DATA....11

IV. METHODS....15

V. RESULTS AND DISCUSSION....23

VI. SUMMARY AND CONCLUSION....45

LIST OF REFERENCES....49

INITIAL DISTRIBUTION LIST....51

THIS PAGE INTENTIONALLY LEFT BLANK

LIST OF FIGURES

Figure 1. PDF and PFA versus Amplitude 2

Figure 2. HUGIN AUV 11

Figure 3. SAS Snippet Example 13

Figure 4. Wavenumber Domain Image 17

Figure 5. SAS snippet at various fractional bandwidths 18

Figure 6. Rock Single Component Distribution PFA Plots 23

Figure 7. Rock Mixture Distribution PFA Plots 24

Figure 8. Gravel Single Component Distribution PFA Plots 24

Figure 9. Gravel Mixture Distribution PFA Plots 25

Figure 10. Sand Single Component Distribution PFA Plots 25

Figure 11. Sand Mixture Distribution PFA Plots 26

Figure 12. Mud Single Component Distribution PFA Plots 26

Figure 13. Mud Mixture Distribution PFA Plots 27

Figure 14. Rock KS and AU Pvalue Heatmap 28

Figure 15. Gravel KS and AU Pvalue Heatmap 29

Figure 16. Sand KS and AU Pvalue Heatmap 29

Figure 17. Mud KS and AU Pvalue Heatmap 30

Figure 18. Rock ρ/CBR/SI Plots 31

Figure 19. Gravel ρ/CBR/SI Plots 32

Figure 20. Sand ρ/CBR/SI Plots 32

Figure 21. Mud ρ/CBR/SI Plots 33

Figure 22. K-K Distribution Rock ρ/CBR/SI Box and Whisker Plots 35

Figure 23. K-K Distribution Gravel ρ/CBR/SI Box and Whisker Plots 36

Figure 24. K-K Distribution Sand ρ/CBR/SI Box and Whisker Plots 36

Figure 25. K-K Distribution Mud ρ/CBR/SI Box and Whisker Plots.....37

Figure 26. K-K Distribution ρ and CBR Rock CI Plots.....39

Figure 27. K-K Distribution ρ and CBR Gravel CI Plots 39

Figure 28. K-K Distribution ρ and CBR Sand CI Plots 40

Figure 29. K-K Distribution ρ and CBR Mud CI Plots.....40

Figure 30. PFA Plots Comparing Homogenous And Non-Homogenous Mud Bottom Types.....41

Figure 31. K-K Distribution Homogenous Mud ρ and CBR CI Plots 42

Figure 32. K-K Distribution Non-homogeneous Mud ρ and CBR CI Plots 42

LIST OF TABLES

Table 1. Parameter Estimation Methods for Each Distribution 19

Table 2. P-Values for Top Performing Distributions For β=1.....30

Table 3. Model Parameters as a Function of β 43

THIS PAGE INTENTIONALLY LEFT BLANK

LIST OF ACRONYMS AND ABBREVIATIONS

AU	Anderson-Darling upper test
CI	confidence interval
CBR	clutter to background power ratio
CDF	cumulative distribution function
EM	expectation maximization
FFI	Norwegian Defense Research Establishment
FFT	fast Fourier transform
G	gamma distribution
GP	generalized-pareto distribution
IFFT	inverse fast Fourier transform
K	k distribution
K-K	k-k distribution
KS	Kolmogorov-Smirnov test
LN	lognormal distribution
MF	match-filtered
ML	maximum likelihood
MoM	method of moments
NURC	NATO undersea research center
PDF	probability density function
R2	Rayleigh 2 component mixture distribution
R3	Rayleigh 3 component mixture distribution
R4	Rayleigh 4 component mixture distribution
R-GP	Rayleigh-generalized-pareto mixture distribution
R-K	Rayleigh-K mixture distribution
R-LN	Rayleigh-lognormal mixture distribution
R-WB	Rayleigh-Weibull mixture distribution
SAS	synthetic aperture sonar
SI	scintillation index
UUV	underwater unmanned vehicle
WB	Weibull distribution

THIS PAGE INTENTIONALLY LEFT BLANK

ACKNOWLEDGMENTS

I would like to thank Roy Hansen and Marc Geilhufe from the Norwegian Defense Research Establishment (FFI) for sharing their SAS data and data processing expertise. I would also like to thank Anthony Lyons from the University of New Hampshire for his recommendations for analyzing resolution dependency for acoustic scattering statistics. Additionally, I would like to thank Mike Cook for all the help he offered me in developing MATLAB code for my figures, as well as advice on data presentation and management.

THIS PAGE INTENTIONALLY LEFT BLANK

I. INTRODUCTION

An issue currently existing in sea-flooring mapping and target detection operations is the difficulty of combing data sets of different resolutions. The reason data sets are not easily integrated together is because synthetic aperture sonar (SAS) data collected at different resolutions will produce probability density functions (PDFs) of the magnitude of the complex pressure which are qualitatively different (Abraham, 2004). This is because as resolution increases, sonar systems are better able to resolve sources of clutter in the environment (by detecting patches of inhomogeneity in seafloors that are unable to be detected at lower resolutions). PDFs are used in target detection operations, as they allow users to identify how likely one is to detect a target. By better resolving sources of clutter, more heavily tailed PDFs at high thresholds are required for target detection operations (Abraham, 2004; Chotiros, 2010). Heavily tailed PDFs are significant for target detection because they translate into higher probability of false alarm (PFA). The top plot in Figure 1 is the PDF versus normalized amplitude of the complex pressure for the Rayleigh and K distributions. The distributions exhibit different behavior such that their peak PDF values are offset from one another (the mode of a K pdf is smaller than the mode of Rayleigh pdf), and that at higher amplitudes the K distribution will always be (even if just slightly) higher than the Rayleigh distribution. The significance of this variance can be seen in the bottom plot of Figure 1. By taking a point on the horizontal axis of the top plot in Figure 1 (for both Rayleigh and K distributions) and integrating out to infinity, one can calculate the PFA. The PFA is plotted in the lower portion of Figure 1. The two plots show that at higher amplitudes, differences in PDF values can result in several orders of magnitude difference in PFA values.

Figure 1. PDF and PFA versus Amplitude

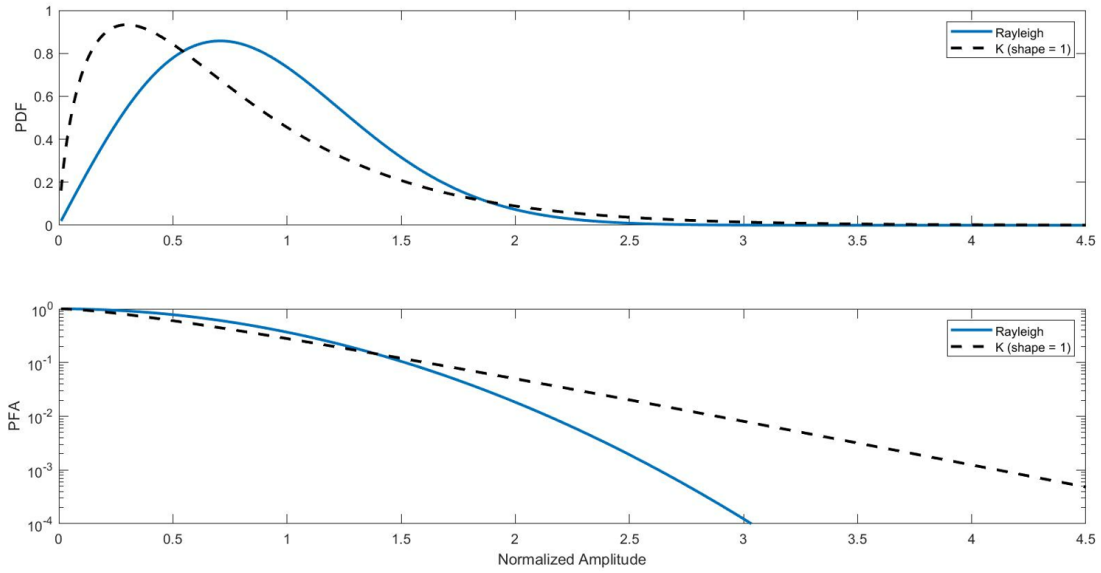

Two plots of PDF and PFA versus normalized amplitude of the complex pressure for the Rayleigh and K distributions. Together these plots show that slight variance in PDF values between distributions will result in several degrees of magnitude difference in PFA values.

Recent technological advancements have exacerbated data integration difficulties. New SAS systems have been designed with larger receiver arrays and better directionality (and therefore narrower bandwidths), which in turn create higher levels of available resolution (Johnson, 2009). Systems that have incorporated these features include the NATO undersea research center (NURC) 300-kHz SAS and the HISAS 1032 (Bellettini, 2009; Hansen, 2011). This means the resolution achieved during target detection operations depends on the specifications of the sonar system being utilized. This resolution disparity creates difficulties in interoperability between partner organizations/nations with different equipment, limits the effectiveness of using multiple types of platforms for a single survey (such as mixing SAS and side scan capable UUVs), and creates difficulties combining newly surveyed data with older recorded data. While research into the resolution dependency of heavy-tailed distributions has occurred, relatively little research has been conducted into the effects of resolution manipulation during the post-processing of high-resolution data from complex seafloor environments. This paper analyzes the effects of gradual resolution reduction, via multi-look methods, on heavy-tailed statistical models. The goal of this research is to enhance sonar perception by modeling how PFA changes

with resolution reduction in order to develop an understanding of how high- and low-resolution sonar data can be combined.

To process the image data, the resolution was manipulated using wavenumber domain filters centered around center frequency and a zero degree look angle. For small spatial bandwidths, multiple sub-looks were used to retain more data (to improve parameter estimation and significance tests). This is because decimation scales with bandwidth reduction, and for small spatial bandwidths, too much data was being discarded to provide meaningful conclusions.

The plots of PFA versus normalized amplitude were selected as the first tool for analysis because PFA is a significant factor in determining target detection operation strategies. False alarms are defined as "threshold crossing peaks in normalized, beamformed, and match-filtered (MF) data that appears at locations not containing an intended target" (Hjelmervik, 2010). None of the images used in this research contain any targets. Therefore, the probability of false alarm for this research is the fraction of samples crossing a set threshold. Mission planners require accurate PFA data to understand the tradeoffs associated with achieving their desired probability of detection (the higher the chosen probability of detection, the higher the number of false targets that will be identified). It is important for mission planners to identify a PFA which is obtainable within their resource limitations, and to understand the man hours or computing power required to sift through the predicted number of identified targets. For this research the PFA was calculated by taking 1 – CDF, where the CDF is the cumulative distribution function associated with the data sets PDF (Strutt, 1919; Olson, 2019). This method was selected because it identifies probability of encountering a signal above a certain threshold, which is more applicable for target detection operations such as mine warfare (Williams, 2017). In this research, the bandwidth of the spectrum will be varied, and analyzed across different seafloor bottom types.

Commonly used single distributions for heavy-tailed statistics were chosen to model the observed data. The single component distributions utilized were the gamma (G), lognormal (LN), Rayleigh (R), Weibull (WB), K, and generalized-Pareto (GP) distributions. The mixture distributions utilized were the K-K mixture (K-K), Rayleigh-

generalized-pareto mixture (R-GP), Rayleigh-K mixture (R-K), Rayleigh-lognormal mixture (R-LN), Rayleigh 2-component mixture (R2), Rayleigh 3-component mixture (R3), Rayleigh 4-component mixture (R4), and Rayleigh-Weibull mixture (R-WB). The equations for the PDFs of each distribution are defined in Chapter IV.

The two goodness of fit tests being implemented for the PFA versus normalized amplitude plots are the Kolmogorov-Smirnov (KS) and Anderson-Darling Upper (AU) tests. It is acknowledged that while the KS test does not prove that a distribution is a good fit, only that it is not a bad fit (Lyons, 1999). The same is also admitted in this paper for the AU. However, they are a tool for identifying several top performing distributions, and are a common method utilized in evaluating target detection performance.

After fitting the distributions to the PFA plots, the top performing distributions were selected for each bottom type by their corresponding p-values (higher p-values indicate better fits to the environmental data). The top performers were then evaluated by how their background and clutter parameters change with resolution reduction. The parameters used for evaluation were the ρ, clutter to background ratio (CBR), and scintillation index (SI) parameters. If a distribution's background and clutter parameters change with resolution manipulation as physically expected, that would indicate the distribution does a good job modeling the physical effects occurring in the environment. Empirical equations were created to model how the parameters change with resolution manipulation, and environmental constants were solved for. Given a desired fractional bandwidth (β) and bottom type, one could then calculate a distribution's ρ and CBR value.

Previous research conducted showed that single distributions often fail to accurately model complex environmental data (Abraham et al., 2011) due to an inflection point in the PFA curve (Olson, 2019). One or more inflection points are caused because in complex seafloors there are multiple features present (such background, clutter, objects of different materials, etc.), and multiple components distributions are needed to accurately model these features (Olson, 2019). Therefore, this paper will focus on analyzing how resolution manipulation via multi-look methods changes single model distribution performance compared to two component mixture models. The goal of this research is to identify physics-based distributions which capture how background/clutter parameters

change with resolution reduction and create rules of thumb allowing one to solve for background and clutter parameters. Higher component non-physics-based models are included to provide a reference point, allowing one to see when there are diminished returns (in terms of distribution fit to environmental data) with added components (higher components are considered non-physical because they contain excess components with no natural explanation for inclusion).

Chapter II provides a summary and analysis of foundational literature. In Chapter III, the high-resolution SAS data used in the analysis is discussed. In Chapter IV, the methods used to process the data and complete goodness of fit comparisons are discussed. In Chapter V, a breakdown of the results is provided. In Chapter VI, the final conclusions and recommendations for future research are summarized.

THIS PAGE INTENTIONALLY LEFT BLANK

II. PREVIOUS LITERATURE

SAS systems have been used for seafloor mapping and target detection operations due to their ability to "produce high resolution images down to centimeter resolution" over hundreds of meters of range (Hansen, 2011). By combining successive pings along a track, SAS systems can increase azimuth resolution (Hansen, 2011). Additionally, by saving multiple pings from a physical aperture, and processing upon completion, a synthetic SAS system creates a larger aperture (Johnson, 2009). This in turn creates an image with constant cross range resolution as a function of range and allows for improved resolution quality at longer ranges (Johnson, 2009). The result is a high-resolution image which allows operators to identify distinct bottom features (Johnson, 2009). Because of the range and resolution associated with SAS systems, it has been recognized as valuable tool for ocean floor related research.

The PDF of pressure backscattered from the seafloor is not Gaussian, and therefore the complex magnitude is non-Rayleigh (Chotiros, 1985). The question is then, what causes this departure, and can it be modeled? Chotiros investigated the role that resolution has in this question, namely beamwidth. By comparing wide beam and narrow beam returns in a plot of the log of the PFA versus mean adjusted backscattering strength, it was shown that resolution effects reverberation returns (Chotiros 1985). While the wide beam returns appeared to follow a Rayleigh distribution, the narrow beam (and thus higher resolution) returns instead more closely followed a log-normal distribution (Chotiros 1985). This research was later expanded on by McDaniel, who utilized the same data set to develop a model for how patchy and/or non-stationary seafloors result in non-Rayleigh statistics (McDaniel, 1990). Her model established that back-scattering strength was dependent upon both the reflection coefficient (a variable dictated by geo-acoustic properties), the grazing angle (which influences penetration and re-scattering), and 2D wave-number elevation spectrum (Johnson, 2019). This model establishes a link between bottom characteristics and backscatter returns, and the interpretation is that non-stationary seafloor roughness properties can result in non-Rayleigh distributions. Of note, this model assumes that the non-stationary roughness lies inside the

sonar resolution, so the model cannot resolve the environment structure like in the research presented here.

Expanding on the study of how bottom characteristics effect backscatter returns, research into how roughness and surface height variations impacted PFA were conducted (Becker, 2004). The results identified that combining backscatter measurements from multiple aspects resulted in a prevalence of heavy-tailed distributions (like the SAS data utilized in this papers experiments) (Becker, 2004). The different mean scattering strength between surfaces was attributed to height distribution properties and the effects of patchy surfaces (Becker, 2004). Related research was also conducted into measuring high-frequency seafloor reverberation to study the difference in scattered amplitude statistics between homogeneous and non-homogeneous bottom types. It was theorized that most seafloor environments (even if not complex) did not have Rayleigh amplitude distributions due to patchiness and clusters of non-homogenous features like shellfish and seagrass (Lyons and Abraham, 1999). The results of these studies proved that the density and strengths of scatterers impacted the amplitude distributions, and that distributions with multiple components were needed to accurately represent seafloor bottom types (Lyons and Abraham, 1999).

Abraham and Lyons also explored the effects of bandwidth and scattering patch on reverberation envelope statistics in a later publication (Abraham and Lyons, 2004). Their research utilizes a non-Rayleigh reverberation model for the K-distribution where the shape parameter is proportional to beamwidth, range, and density of seafloor scattering patches, but inversely proportional to bandwidth (Abraham and Lyons, 2002). The model described above was modified to account for reverberation envelop dependency when calculating the size and number of the scattering patches in relation to the sonar-resolution cell (Abraham/Lyons, 2004). This was done to account for an observed "trend back toward a Rayleigh reverberation" distribution for high shape parameter and bandwidth values (contradicting the original model) (Abraham/Lyons, 2004). Their theory was that the contradiction was caused due to over-resolving patches in range but not angle (Abraham/Lyons, 2004). Their results show reverberation envelope statistics, specifically the resulting reverberation distribution (whether Rayleigh or non-Rayleigh) is dependent on resolution (which is related to bandwidth).

Abraham's later research also explored the need for mixture models. He evaluated environments high degrees of scattering due to the presence of clutter derived from rock outcrops, seaweed, fish, and mud-volcano fields (Abraham, 2011). When analyzing seafloors with stationary (non-moving) and nonstationary (moving, like schools of fish) clutter, it was shown that the environmental PFA curve will develop a "knee," where the clutter response distribution will dominate above the knee (resulting in higher tail distributions), and background distribution will dominate below the knee (Abraham 2011). Applying the K-S and AU tests to the data, it was shown that two component mixture models have better distribution fits than the single component mixture models (Abraham, 2011). This is because the two component models better account for the overlap in sonar data between clutter and diffused background (Abraham, 2011). Further research into mixture models was conducted to identify the connections between statistical parameters and environmental parameters (Olson, 2019). This research was conducted to identify not only mixture distributions that fit environmental PFA curves well, but also had a physics-based explanation. The results were that for rocky outcrops the K-K mixture was the top performing distribution not only for its high p-values, but also because its values of ρ matched closely with the expected physical effects based on sonar imagery, and because the distribution's equation is connected to scattering physics (Olson, 2019). The R-GP and R-LN were the next best performing distributions.

The above literature establishes how SAS data can be applied to target detection and seafloor mapping operations, how sonar resolution is dependent upon bandwidth, how higher resolution leads to non-Rayleigh distributions/higher tailed PFA plots, how bottom characteristics effect scattering statistics/PFA, and how two component physics-based mixture models are needed to adequately model higher resolution data due to their higher tailed distributions. What has not been studied in depth are the effects of resolution manipulation during the post-processing of high-resolution data from complex seafloor environments. This paper will use a large data set to identify the top performing physics-based distributions for multiple bottom types and analyze how those distributions perform during post-processing resolution reduction. The goal of this paper is to develop an understanding how high and low- resolution data can be linked through a model and its parameters.

THIS PAGE INTENTIONALLY LEFT BLANK

III. DATA

Seventeen high resolution SAS images were analyzed in this paper. The data for all seventeen images were collected by the Norwegian Defense Research Establishment (FFI) in March 2017. The data was collected by a HISAS 1032 interferometric SAS system carried by FFI's HUGIN HUS AUV (Sæbø, 2007). Figure 2 is an image of a HUGIN AUV. All the SAS were taken from western Norway outside the city of Bergen. The survey lines for the seventeen images were chosen because they were complex seafloors with relatively rough terrain.

Figure 2. HUGIN AUV

A picture of a HUGIN AUV, the system used to collect this experiments data. Source https://www.hydro-international.com/content/news/swire-seabed-orders-hugin-autonomous-underwater-vehicle.

The vehicle altitude during the surveys was approximately 30m. The SAS center frequency utilized for data collection was 100 kHz, and the bandwidth was 30 kHz (Sæbø, 2007). After collection the SAS images were constructed using a back-projection algorithm, where an estimated render plane based on side-scan bathymetry is used (Hansen, 2011). The theoretical resolution in the images is approximately 3.7 cm along-track and 3.2 cm cross-track.

The seventeen SAS images provided by FFI contain images with complex shapes of varying scales. The SAS images were curated high-quality images relatively free from navigational uncertainty. For analysis, the SAS images were divided into homogenous bottom type snippets (Rock, Gravel, Sand, and Mud) in the space domain. Figure 3 is an example of how a SAS image was subdivided into different bottom types. The snippets were chosen to encompass a large range of shapes, sizes, and features to in order to develop general rules of thumb for analysis. As such, this paper does not have a standard snippet size. 380 snippets were taken between all seventeen SAS images (138 rock, 82 gravel, 86 sand, and 74 mud snippets). The number of snippets taken per image was not equal, but instead dependent on how diverse the topography of each image was.

Figure 3. SAS Snippet Example

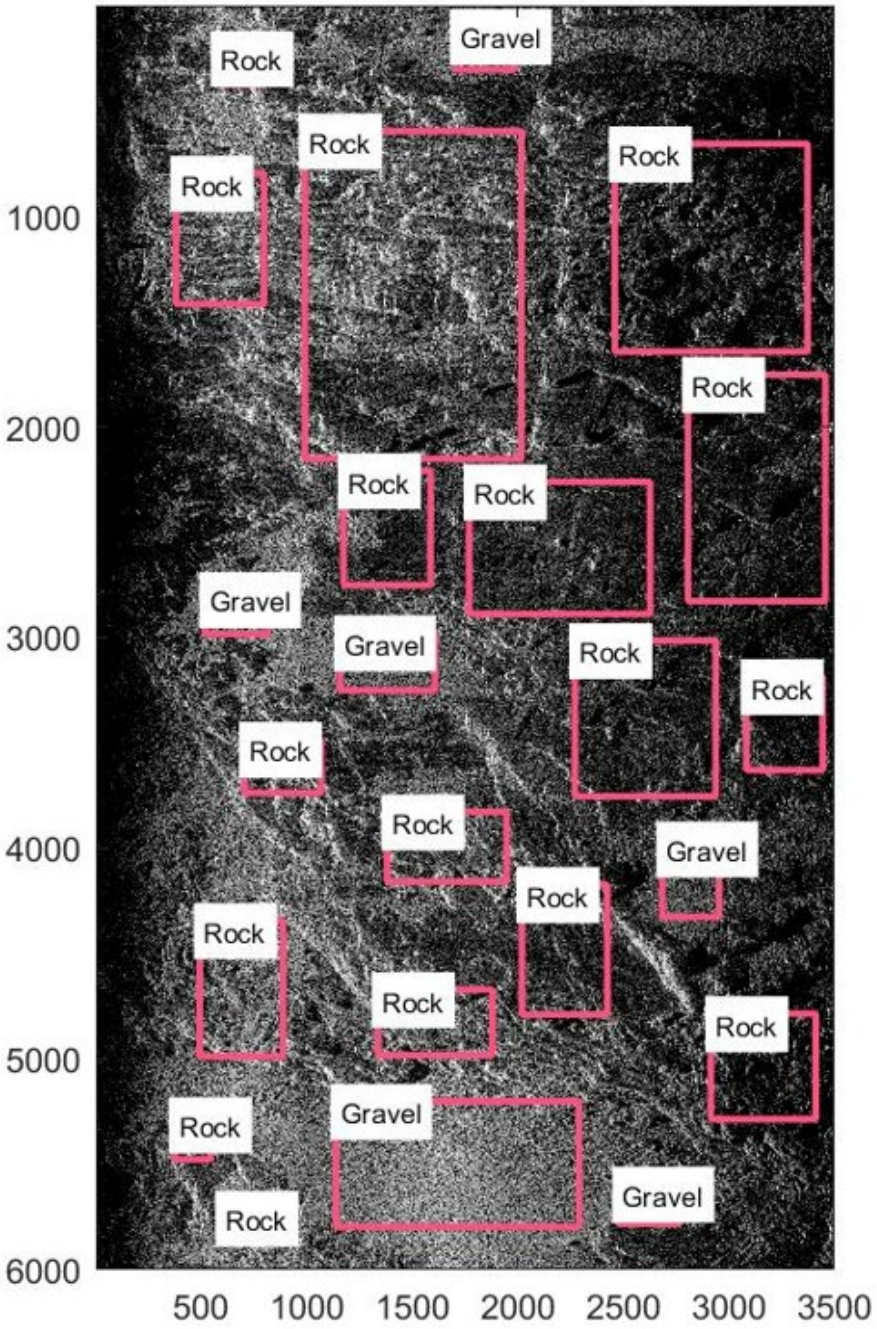

An example of one of the seventeen SAS images subdivided into snippets by homogeneous bottom types. Pixel resolution is 2cm per pixel. The above image is 120 by 70 meters.

THIS PAGE INTENTIONALLY LEFT BLANK

IV. METHODS

This section will discuss the mathematical equations and process used for this paper's analysis. First the equations for the distributions used for goodness of fit evaluation are provided. Second, the methods used for data processing and resolution reduction are discussed. Third, the parameter estimation methods are discussed. Fourth, how the p-value goodness of fit analysis was conducted is explained. Fifth, the equations used for calculating the clutter and background parameters are provided. Sixth, is a discussion on how the background and clutter parameter analysis was conducted. Lastly, how the empirical equations and environmental constants (to solve for ρ and CBR) were derived is explained.

The PDF of the Gamma distribution was the same specific form as utilized by Abramowitz and Stegun (1970). The Rayleigh, K, Weibull, GP, and log-normal PDF specific forms were the same as utilized Olson et al. (2019). The PDF of the Rayleigh distribution is:

$$f(x) = 2x/(\lambda)e^{(-\frac{x^2}{\lambda})}, \tag{1}$$

where $x > 0$ is the amplitude, and $\lambda > 0$ is the scale parameter. The gamma distribution PDF is:

$$f(\mathrm{x};\varphi,\lambda) = \frac{2x}{\Gamma(\varphi)}x^{2(\varphi-1)}e^{\frac{-\mathrm{x}^2}{\lambda}}, \tag{2}$$

where φ > 0 is the shape parameter, and λ>0 is the scale parameter, and Γ is the gamma function (Abramowitz, 1970). The K distribution PDF is:

$$f(x) = 4/(\sqrt{\lambda}\,\Gamma(\alpha))(x/\sqrt{\lambda})^{\alpha}K_{\alpha-1}\left[\frac{2x}{\sqrt{\lambda}}\right], \tag{3}$$

where $\alpha > 0$ is the shape parameter, $\lambda > 0$ is the scale parameter, and K is the modified Bessel function of the second kind (Abramowitz, 1970). The Weibull distribution PDF is:

$$f(x) = 2\beta x^{2\beta-1} / \left(\lambda^{\beta}\right) e^{-\left(\frac{x^2}{\lambda}\right)^{\beta}}, \tag{4}$$

where $x > 0$ is the amplitude, $\beta \epsilon [0, 1]$ is the shape parameter, and $\lambda > 0$ is the scale parameter. The PDF of the GP distribution is:

$$f(x) = 2x / \left(\lambda(1 + \gamma x^2 \lambda^{-1})^{\gamma^{-1}+1}\right), \tag{5}$$

where $x > 0$ is the amplitude, γ is the shape parameter, and $\lambda > 0$ is the scale parameter. The PDF of the log-normal distribution is:

$$f(x) = 2/\left(x\sigma\sqrt{2\pi}\right) e^{-\left(2\,log\left(\frac{x}{\lambda}\right)\right)^2/(2\sigma^2)}, \tag{6}$$

where $\sigma > 0$ is the shape parameter, and $\lambda > 0$ is the scale parameter.

After the snippets were defined, the data's resolution was gradually reduced to understand the resolution dependence of the PDF for each bottom type. To accomplish this, the space domain was converted into the wavenumber spectrum by applying an FFT in 2 dimensions. The wavenumber spectrum data was equalized by calculating an estimate of the spectral weighting using a size 20 pixels x 20 pixels square low pass smoothing filter applied to the complex magnitude wavenumber domain and dividing the complex data by the smooth magnitude estimate. The equalization was performed in order to control the tapering for each subregion.

Figure 4. Wavenumber Domain Image

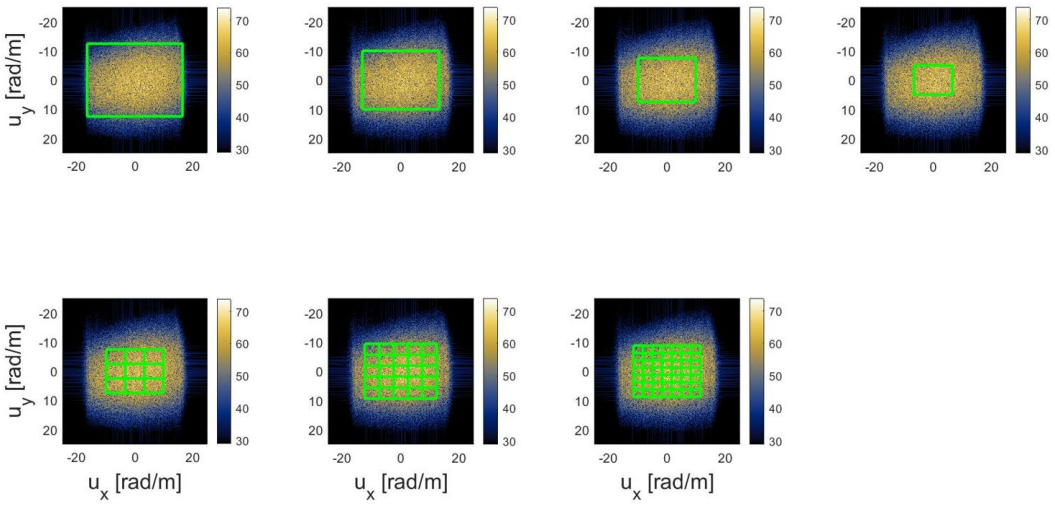

From top left to top right and then bottom left to bottom right, an example of a snippet after conversion to the wavenumber spectrum, and gradual division of the spectrum by β (1, .8, .6, .4, .2, .15, .1). Equalization was not applied to these images.

After the data was equalized, a bandpass filter was applied to reduce the resolution. For this paper the equation for β is:

$$\beta = \frac{BW}{f_0} \tag{7}$$

where BW is the bandwidth and f_0 is the center frequency. A β of 1 (no reduction), 0.8, 0.6, 0.4, .3, .2, .15 and 0.1 were used in this paper. Initially, the resolutions were reduced using a standard multilook. However, standard multilook analysis reduces resolution using a harmonic series (e.g., 1/2, 1/3, 1/4, etc.), which creates a large gap between the highest bandwidth and the next highest bandwidth. The goal was to reduce resolution gradually and fractional bandwidths (β) better accomplished this. Therefore, for a resolution reduction equivalent to a multi-look of 3 (in both directions), a snippet that is 1/9 the area of the wavenumber spectrum based off the center is retained. The exception is for multi-look fractions of .2 and below. For data analyzed with low fractional bandwidths a larger portion of the wavenumber domain is preserved by using multiple non-overlapping bandpass filters to maintain at least 50% of the wavenumber spectrum in each dimension. This is because for reduced resolution, the number of independent samples is smaller than

that of the original resolution image. Once the multi-look resolution reduction was complete the data was converted from the wavenumber spectrum back to the space domain by the way of an inverse FFT (IFFT). After the IFFT was applied the data was decimated by a factor of 6 divided by β to ensure the resulting data was independent of one another.

Figure 5. SAS snippet at various fractional bandwidths

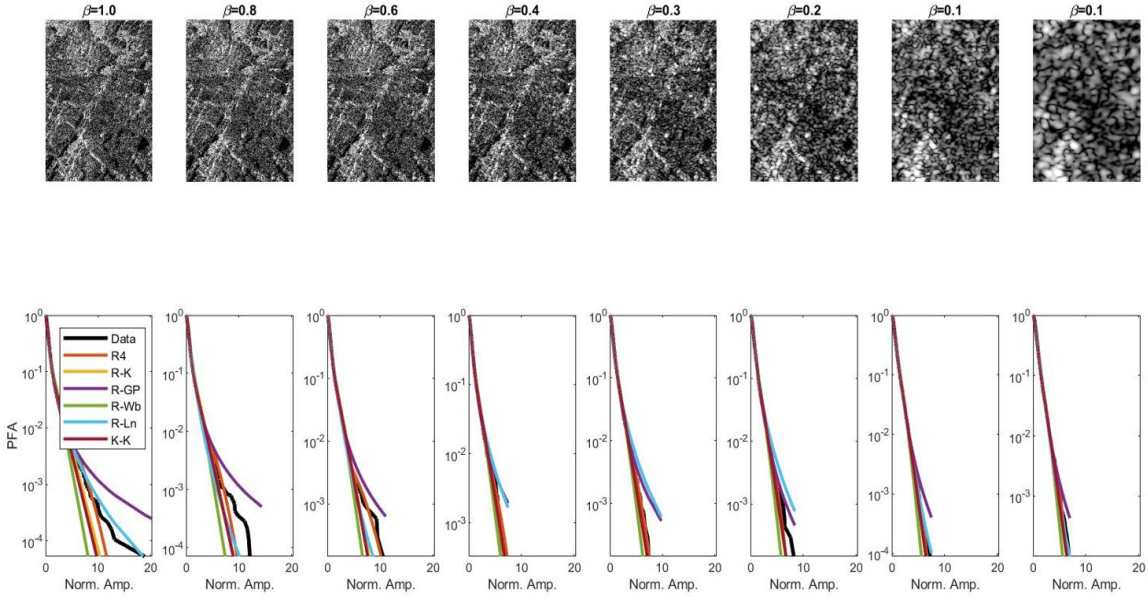

Comparison of rock snippet image and PFA with gradual resolution reduction (from left to right, 1, 0.8, 0.6, 0.4, 0.3, 0.2, 0.15, 0.1).

After decimation is complete the snippet data is converted into a column vector. Results were then grouped by bottom type. After data organization PFA plots for single and mixture distributions were generated in order to compare K-S and AU goodness of fit results for all resolutions. The KS test statistic is a "nonparametric measure that describes how well a theoretical cumulative distribution function (CDF) fits the CDF estimated from observed data" (Lyons, 1999). The AU test statistic "emphasizes the upper tails of the distribution and is based on an average squared distance between the data and the model" (Olson, 2019). To summarize the results of the PFA goodness of fit results, heatmap plots and box-whisker plots were produced. In addition to heatmap and box-whisker plots for

the KS p-values, plots of the AU p-values were also produced. This was done to verify each distributions performance in the upper tail of the PDF plot, which is the area of most importance for this research.

Table 1 summarizes the parameter estimation techniques utilized for each distribution. For the single models, the maximum likelihood (ML) method was employed, except for the K distribution, which used the method of moments (MoM). The ML method either uses an analytic or numerically search for the parameters that maximize the likelihood function. It is unbiased and offers the lowest uncertainty. The MoM is used for the K distribution both because the ML parameter estimates are not available in closed form, and that derivatives of the likelihood function are numerically unstable making it difficult to implement a numerical maximization (Abraham 2010). For the mixture models, the expectation maximization (EM) method is utilized. The EM method separates data into two groupings, background and clutter, and estimates the parameters for each component of the mixture separately. With improved parameter estimates, better estimates of the probability that each data sample belongs to each component can be made. The method repeats until the parameters do not change below a given threshold of each distribution to develop its parameters. EM is independent of method of parameter estimation. One can use anything for the "maximization" step, such ML, MoM, or something else. For the other mixture models, only the background component is calculated through the EM method. The K-distribution uses the MoM to calculate the clutter probability. The K-K distribution utilizes maximum likelihood to calculate both parameters. The rest of the mixture distributions utilize EM for the background, and the gradient for the clutter.

Table 1. Parameter Estimation Methods for Each Distribution

	Distribution	Estimator Method
Single Models	Rayleigh	Maximum Likelihood
	K	Method of Moments
	Gamma	Maximum Likelihood
	Lognormal	Maximum Likelihood
	Weibull	Maximum Likelihood
	Generalized Pareto	Maximum Likelihood

	Distribution	Estimator Method
Mixture Models	Rayleigh (4 Component)	Expectation Maximization (ML)
	Rayleigh (3 Component)	Expectation Maximization (ML)
	Rayleigh (2 Component)	Expectation Maximization (ML)
	Rayleigh-K	Expectation Maximization + (ML/MoM)
	Rayleigh-Generalized Pareto	Expectation Maximization + (ML / ML gradient)
	Rayleigh-Lognormal	Expectation Maximization + Gradient
	Rayleigh-Weibull	Expectation Maximization + Gradient
	K-K	Brute force Maximum Likelihood

After calculating the p-values for each distribution, the top performing physics-based distributions were identified and analyzed by background and clutter parameters. This additional stage of analysis is conducted because as mentioned earlier, p-values do not guarantee the distributions fit the environment well (have physics-based reasons for their high degrees of fit). Analysis of how distributions fit environmental parameters is needed to identify if distributions are physics-based solutions. Therefore, the remaining distributions were evaluated using the ρ, Clutter to Background Power Ratio (CBR), and Scintillation Index (SI) parameters. ρ is a dimensionless parameter that is the fraction of background pixels compared against the fraction of clutter pixels (so a value of 1 indicates all pixels are background, a value of zero indicates all pixels are clutter, and a value of .5 indicates there's an even distribution between background and clutter pixels). The equation for ρ for the PDF of a mixture distribution is:

$$p(x|\theta_0, \rho, \theta_1) = \rho\rho_0((x|\theta_0) + (1 - \rho)p_1(x|\theta_1) \quad (8)$$

where $p_0(x|\theta_0)$ is the background PDF, $p_1(x|\theta_1)$ is the clutter PDF, and ρ is the mixing proportion (Olson, 2019). CBR is a dimensionless parameter measured that is the ratio of clutter intensity over background intensity (so a high number would indicate that the clutter intensity is much more significant than the background intensity). The equation for CBR is:

$$CBR = \frac{\int dx\ x^{\,2} p_1(x|\theta_1)}{\int dx\ x^2\ p_0(x|\theta_0)} \tag{9}$$

where $p_0(x|\theta_1)$ is the clutter PDF, $p_1(x|\theta_0)$ is the background PDF, and x is the envelope (Olson,2019). SI is a dimensionless parameter that measures how strongly tailed a distribution is (so a value of 1 would be Rayleigh, and a value significantly higher than one would indicate a very strongly tailed distribution). The equation for SI is:

$$SI = \frac{< x^4 > - < x^2 >^2}{< x^2 >^2} \tag{10}$$

where x is the envelope of the PDF (Jackson, 2007). The ρ and CBR plots were generated around the data set's median instead of mean. This is because outliers, especially for CBR values, had the potential to be significantly higher than most data points. Therefore, using mean values for the plots and visual aids would not have accurately reflected each distributions fit performance (or data would have needed to be thrown away to ensure trends were represented accurately). By using the median instead, no data had to be thrown away to successfully illustrated the data trends.

The top performing distributions were analyzed to see if the background and clutter parameters change with resolution reduction in line with a physical explanation. The expected outcome for ρ was to see a decrease in values with resolution reduction, as the scatterers become less defined and the pixels that contain clutter would increase in proportion to the pixels containing background. The expected outcome for CBR was for it

to decrease with resolution reduction, but to remain high (well above 1), as clutter intensity remains more prevalent than background intensity even with significant resolution reduction. The expected outcome for SI is for the value to become more Rayleigh like, approaching closer to one with increased resolution reduction. After verifying that the top performing distributions background and clutter parameters change as physically anticipated, the top distribution was plotted as a function of ρ and CBR and fitted with confidence intervals reflecting a 95% probability. The confidence interval was calculated by using the bootstrap method employed by Davison and Hinkley (1997). Bootstrap method is a way of estimating a desired parameter by averaging approximations from multiple samples (Davison, 1997). The ρ and CBR confidence interval plots were also each fit with an empirical equation to capture how the background and clutter parameters change with resolution reduction. Empirical equations 12 and 13 were developed through trial and error of various equations, based on observed data trends, to determine how to best calculate the ρ and CBR values. The empirical equations are:

$$\rho = a_1 \frac{log(\beta)}{\beta} + b_1 \tag{12}$$

$$CBR = a_2 \frac{log(\beta)}{\beta} + b_2 \tag{13}$$

where a and b are constant values needed to solve for ρ or CBR (bottom type dependent, see Table 3), and β is the fractional bandwidth. From the empirical equations, constant parameters were calculated for each bottom type and put into a table. The formulated equation and environmental constant values are described in detail in Chapter V. By using an empirical fit, rules of thumb were developed for how resolution affects the statistical distribution of sonar data, the first step in identifying if data collected with different sensor systems (and different resolutions/bandwidths) can be combined.

V. RESULTS AND DISCUSSION

Figures 6–13 display PFA versus normalized amplitude for 12 snippets of the 380 analyzed during this project. From visual analysis, significant trends in the data are evident. For the single distributions, the GP and LN distribution tend to overestimate the PFA across all bottom types. The Rayleigh, Weibull, and the K distributions tend to underestimate the PFA across all bottom types. Additionally, all the single distributions fit to the environmental data improves with resolution reduction, except for the LN distribution. This is because as the resolution is reduced, the shape of the environmental line becomes more Rayleigh like (concave down). The LN distribution cannot fit a Rayleigh curve, and thus its fit does not improve with resolution reduction. For the mixture distributions, almost all fits across all bottom types were better than the performances of the single component distributions. There were no obvious trends in the data regarding overestimating or underestimating the PFA, and all mixture distributions fits improved with resolution reduction. Because the mixture distributions fits were much closer, heatmaps of the p-values were required to identify the top performing distributions.

Figure 6. Rock Single Component Distribution PFA Plots

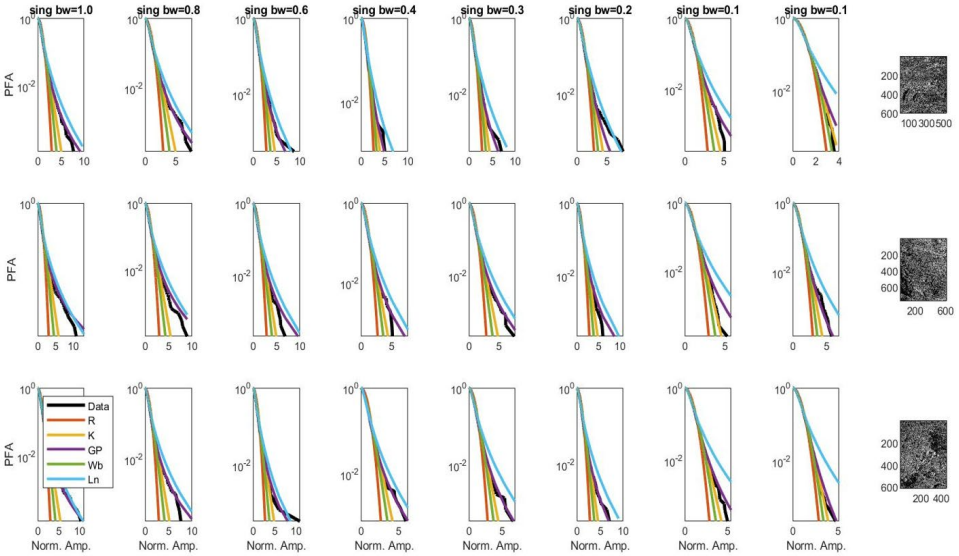

PFA plots for 12 snippets, three snippets per bottom type. Each row (top, middle, bottom) for the single component and mixture PFA plots correspond to the same snippet.

Figure 7. Rock Mixture Distribution PFA Plots

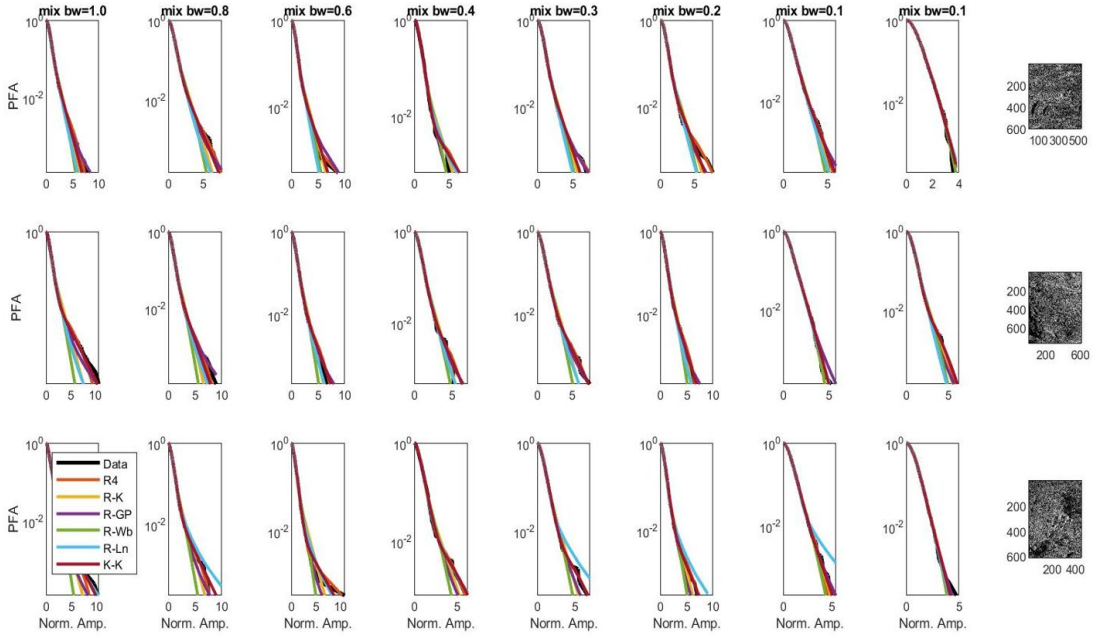

PFA plots for 12 snippets, three snippets per bottom type. Each row (top, middle, bottom) for the single component and mixture PFA plots correspond to the same snippet.

Figure 8. Gravel Single Component Distribution PFA Plots

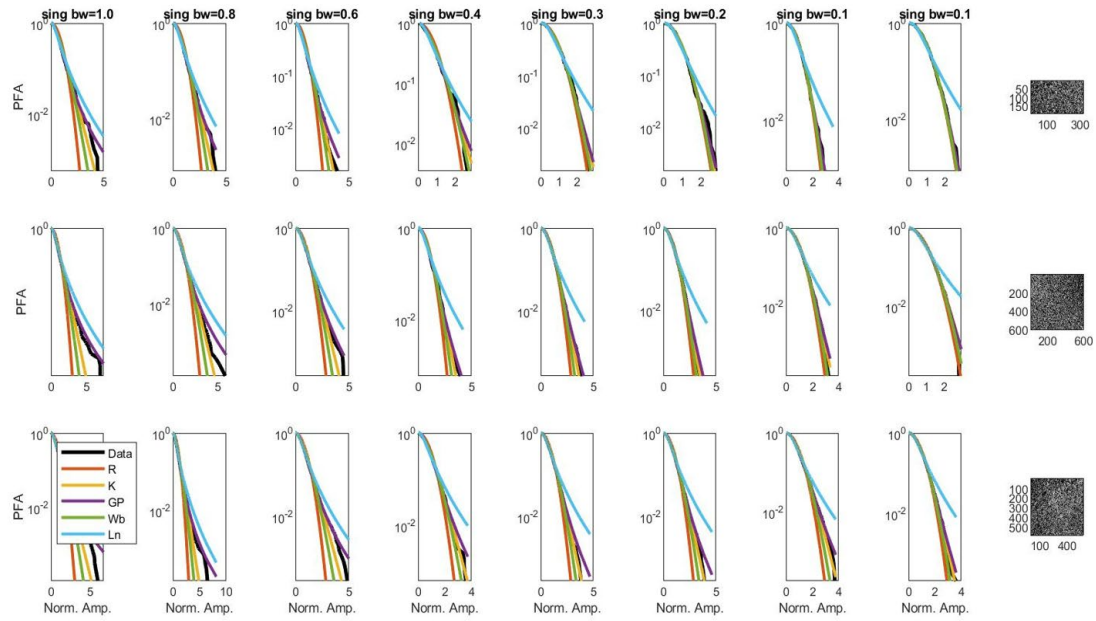

PFA plots for 12 snippets, three snippets per bottom type. Each row (top, middle, bottom) for the single component and mixture PFA plots correspond to the same snippet.

Figure 9. Gravel Mixture Distribution PFA Plots

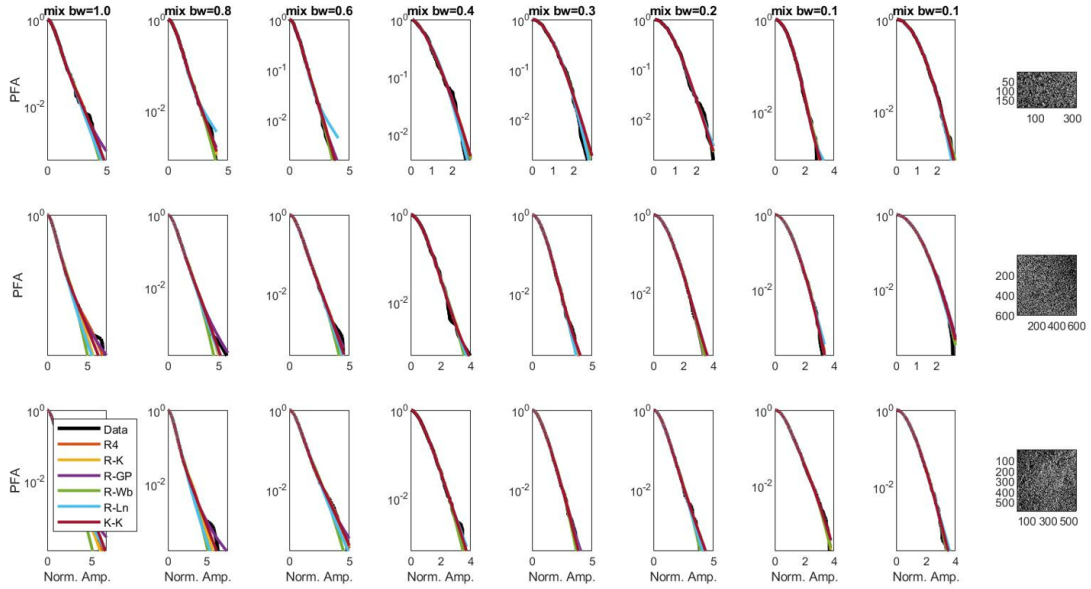

PFA plots for 12 snippets, three snippets per bottom type. Each row (top, middle, bottom) for the single component and mixture PFA plots correspond to the same snippet.

Figure 10. Sand Single Component Distribution PFA Plots

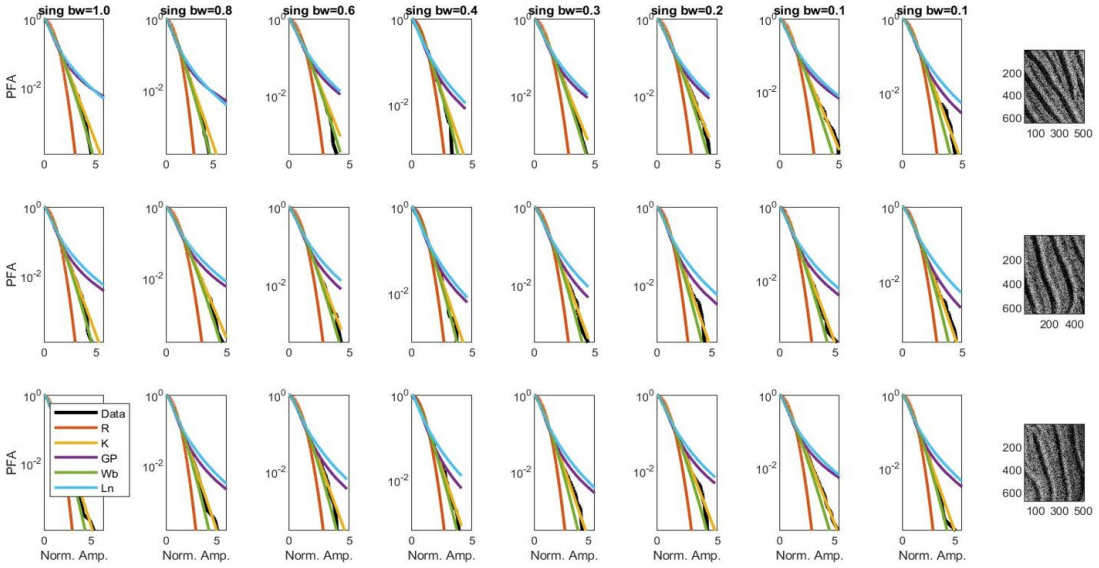

PFA plots for 12 snippets, three snippets per bottom type. Each row (top, middle, bottom) for the single component and mixture PFA plots correspond to the same snippet.

Figure 11. Sand Mixture Distribution PFA Plots

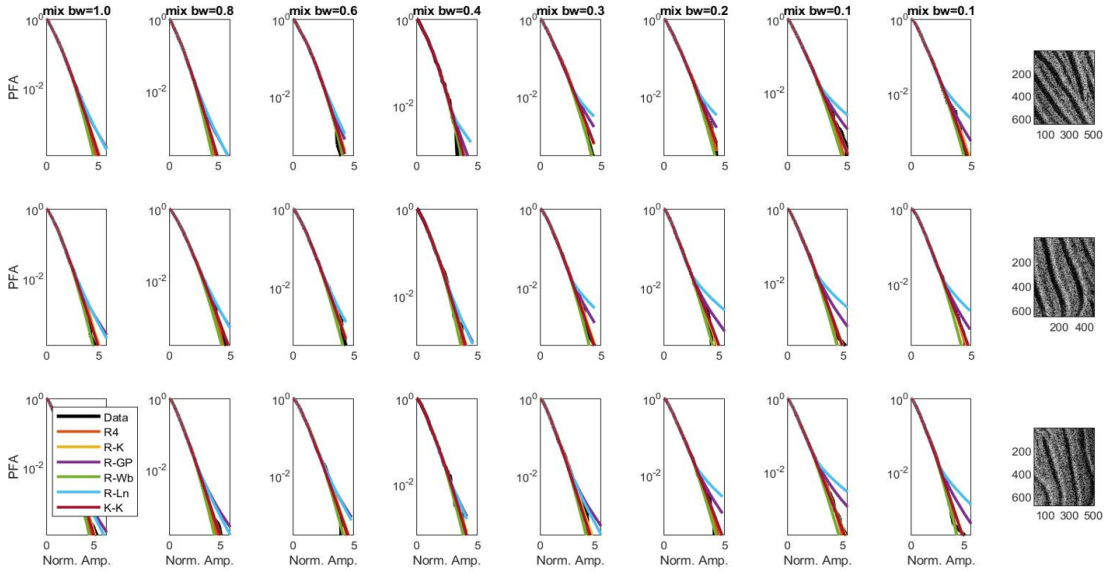

PFA plots for 12 snippets, three snippets per bottom type. Each row (top, middle, bottom) for the single component and mixture PFA plots correspond to the same snippet.

Figure 12. Mud Single Component Distribution PFA Plots

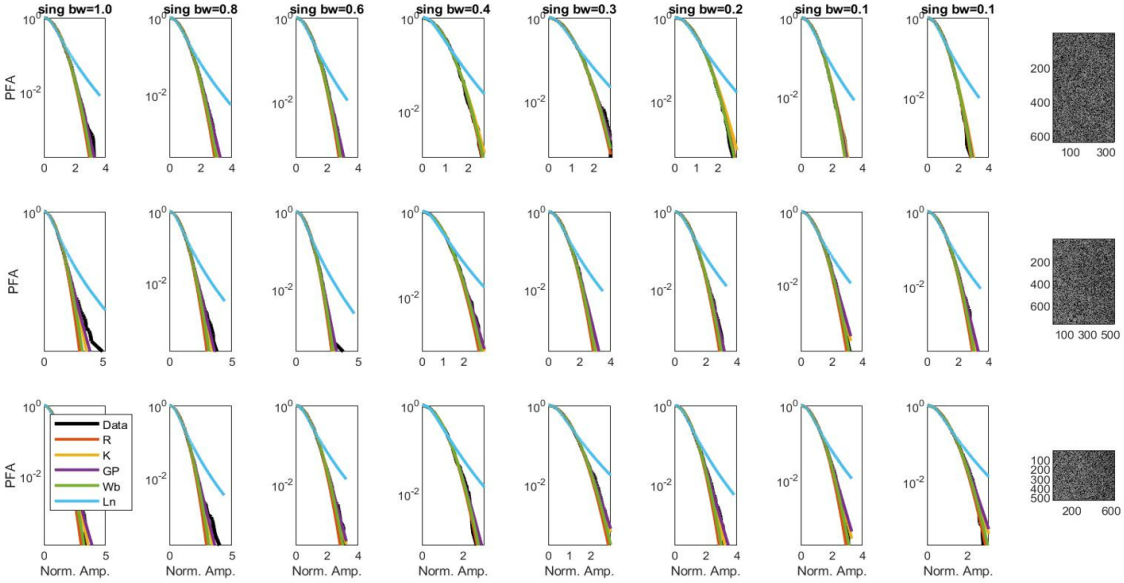

PFA plots for 12 snippets, three snippets per bottom type. Each row (top, middle, bottom) for the single component and mixture PFA plots correspond to the same snippet.

Figure 13. Mud Mixture Distribution PFA Plots

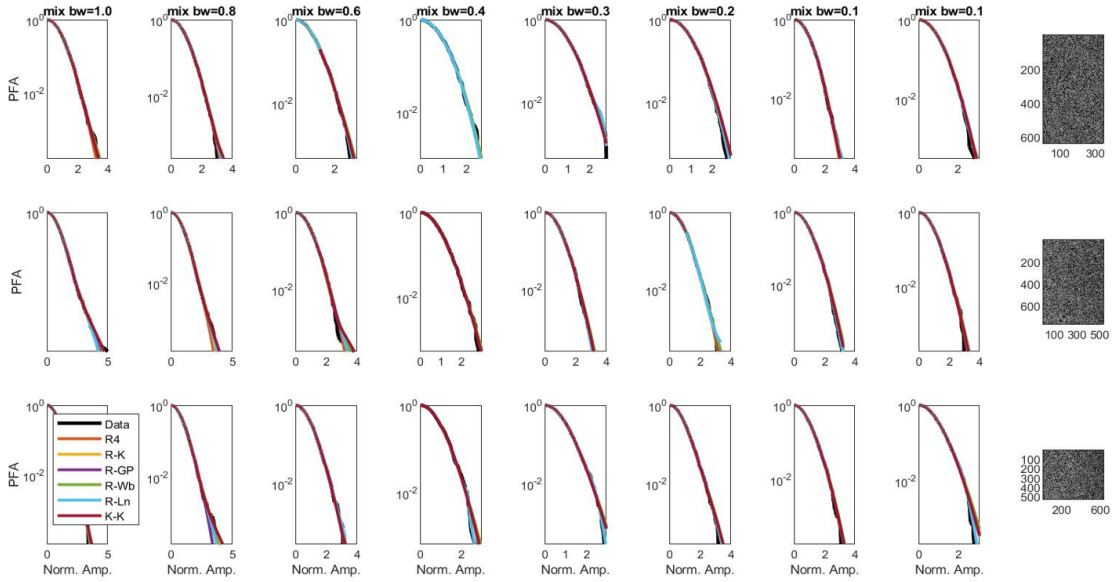

PFA plots for 12 snippets, three snippets per bottom type. Each row (top, middle, bottom) for the single component and mixture PFA plots correspond to the same snippet.

Figures 14–17 are heatmaps summarizing the performance (captured by the p value of the KS or AU statistical test) of each model distribution for each bottom type per fractional bandwidth. From these tables the top performing physics-based distributions were selected for background and clutter evaluation. For example, although the Rayleigh-Mixture 4 and the Rayleigh-lognormal mixture were two of the top performing distributions for rocky seafloors, those distributions have no physical explanation for how they model the physical environmental parameters (The R4 would be a physics-based model if 4 different types of scattering were occurring, but for most bottom types there are only two types occurring). Therefore, these distributions were excluded from further analysis. The R4 distribution was instead used as measuring stick (because it was the distribution with the most components), to see how much accuracy is obtained by using additional components. If a two-component mixture model performed similarly to the R4 model, that was an indication that the two-component model accurately modeled the environmental data. For example, the K-K distribution p-values for mud were nearly equal to the R4 distribution's p-values, which in turn validated the conclusion that the K-K distribution accurately fit the environmental data. After comparing the distribution's p-

values against one another, the K-K and the Rayleigh-GP mixtures were selected as the top performing physics-based distributions. Table 2 summarizes the K-K and R-GP p-values at a β of 1. Of note, the GP distribution performed the best amongst the single component distributions. However, the GP distribution only had a P-value greater than .3 throughout all resolutions in the mud bottom type. The poor fitting of single distributions reinforces the theory discussed in the previous literature section, that multiple component distributions are needed to accurately model complex seafloor performances (Abraham, 2011). Therefore, no single distributions were carried over to the next stage of analysis, evaluating background and clutter parameters.

Figure 14. Rock KS and AU Pvalue Heatmap

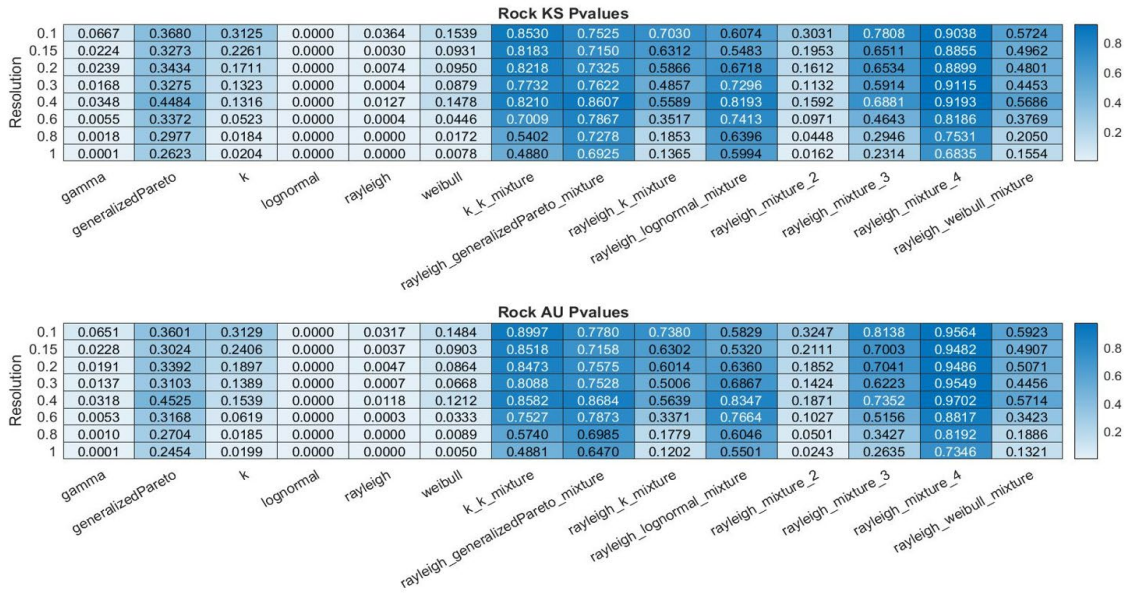

Heatmaps for each bottom type for all β.

Figure 15. Gravel KS and AU Pvalue Heatmap

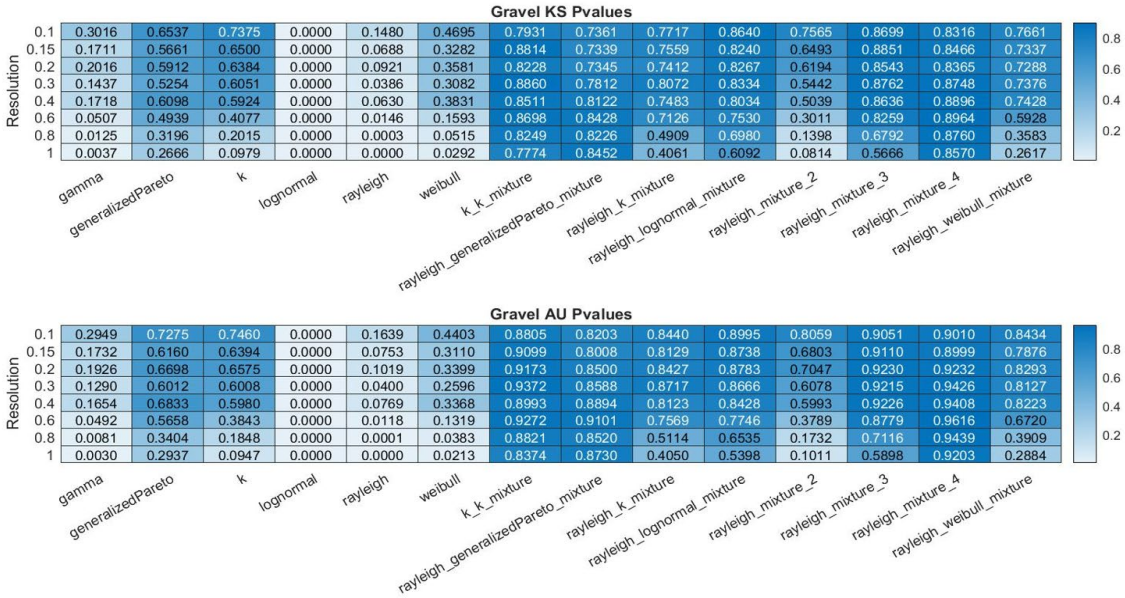

Heatmaps for each bottom type for all β.

Figure 16. Sand KS and AU Pvalue Heatmap

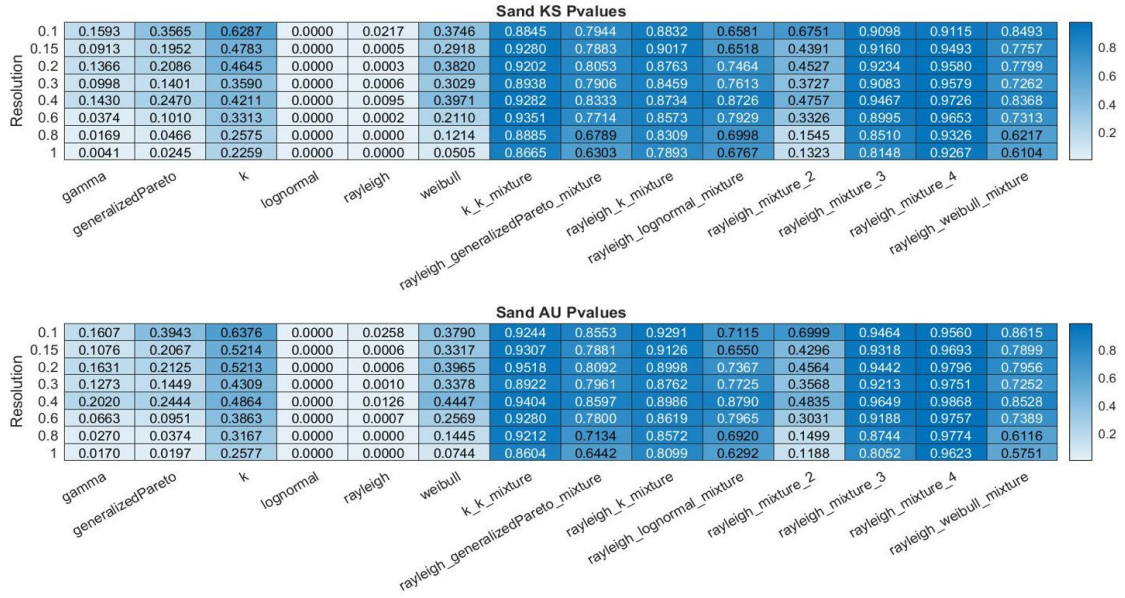

Heatmaps for each bottom type for all β.

Figure 17. Mud KS and AU Pvalue Heatmap

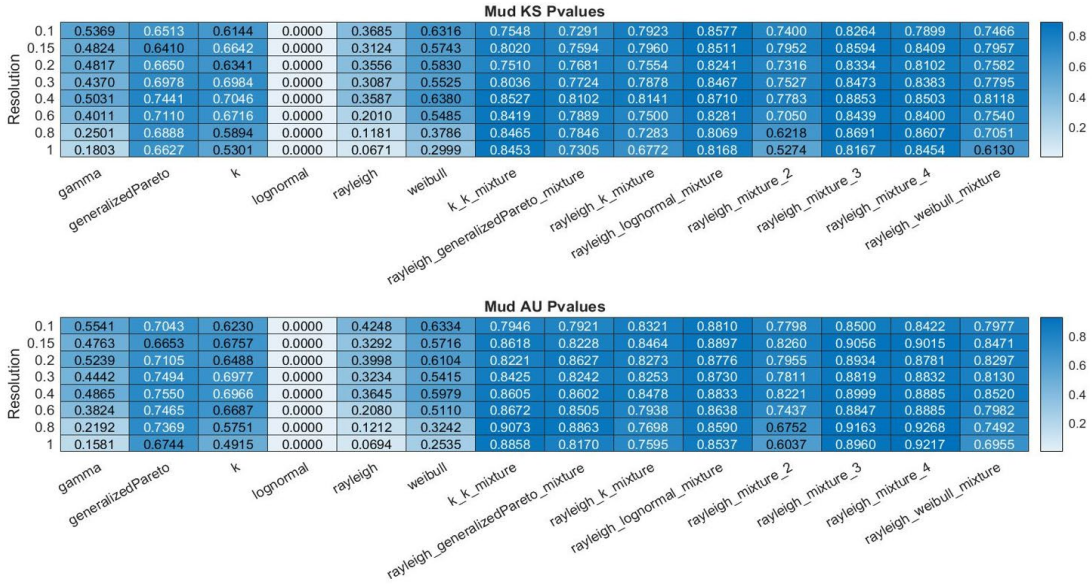

Heatmaps for each bottom type for all β.

Table 2. P-Values for Top Performing Distributions For β=1.

Bottom Type	Distribution	P-Value Fit (AU)	P-Value Fit (KS)
Rock	Rayleigh-GP Mixture	.6470	.6925
	K-K Mixture	.4881	.4880
Gravel	Rayleigh-GP Mixture	.8730	.8452
	K-K Mixture	.8374	.7774
Sand	Rayleigh-GP Mixture	.6442	.6303
	K-K Mixture	.8604	.8665
Mud	Rayleigh-GP Mixture	.8170	.7305
	K-K Mixture	.8858	.8453

Because good p-value returns alone do not guarantee distributions fit the environmental data well, another analysis of the top performing p-value distributions was conducted. Figures 18–21 show the median ρ and CBR values for each β value per bottom type, as well as the associated SI values. The SI values are bottom type dependent (as opposed to distribution dependent), and thus all distributions have the same SI values for each bottom type. Comparing Figures 18–21, one can see the range in how heavy-tailed

each bottom type is for each β value. As expected, the rock bottom type is by far the most heavy-tailed bottom type (indicated by the high SI values at higher resolutions), due to the large amount of scatters present. However, the other bottom types are also very heavily tailed, with SI values much greater than 1 for most β values. For all bottom types we see a trend where the data becomes less heavily tailed with resolution reduction. While the data becomes more Rayleigh like with increased resolution reduction, the data never becomes fully Rayleigh (meaning the SI values never settle at a value of 1).

Figure 18. Rock ρ/CBR/SI Plots

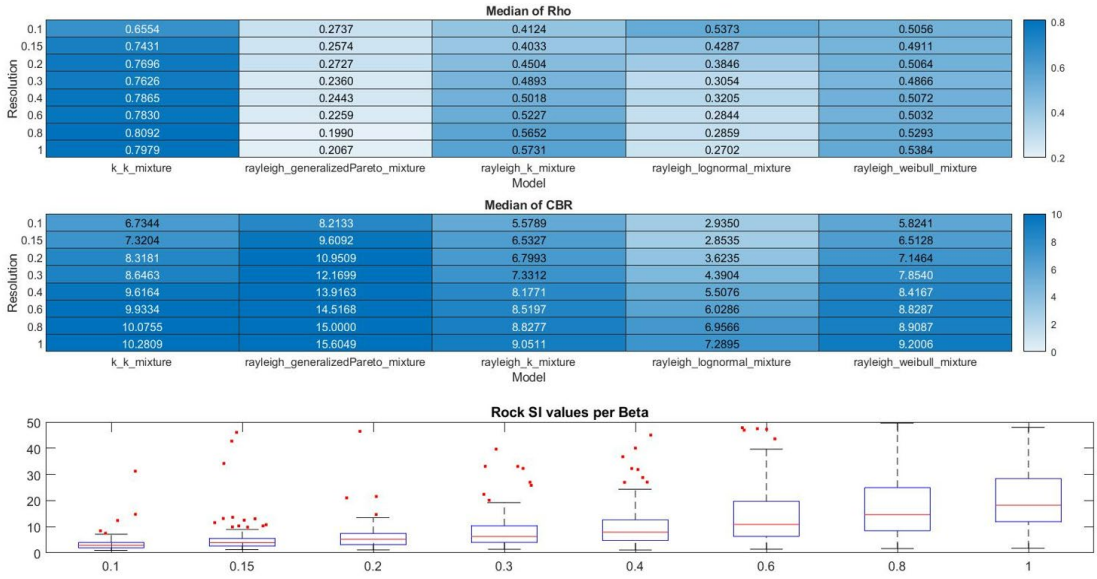

Figure 19. Gravel ρ/CBR/SI Plots

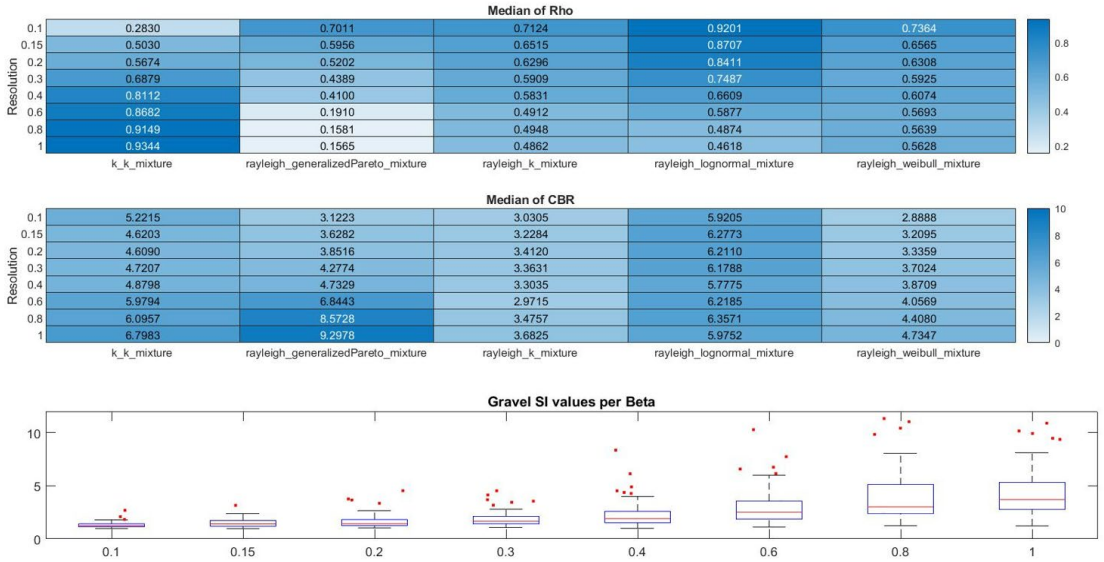

Figure 20. Sand ρ/CBR/SI Plots

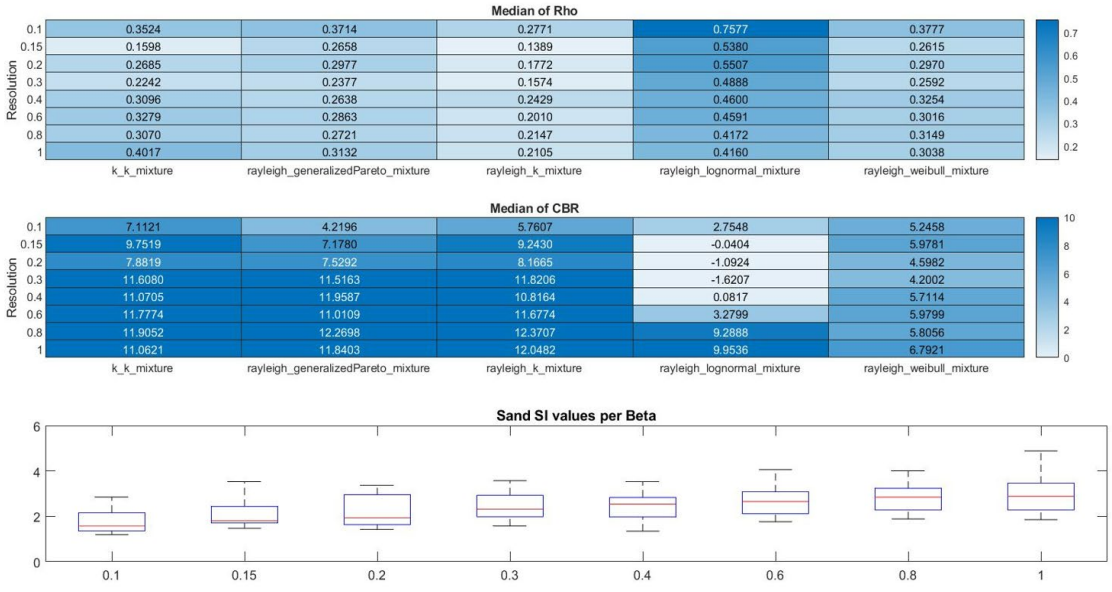

Figure 21. Mud ρ/CBR/SI Plots

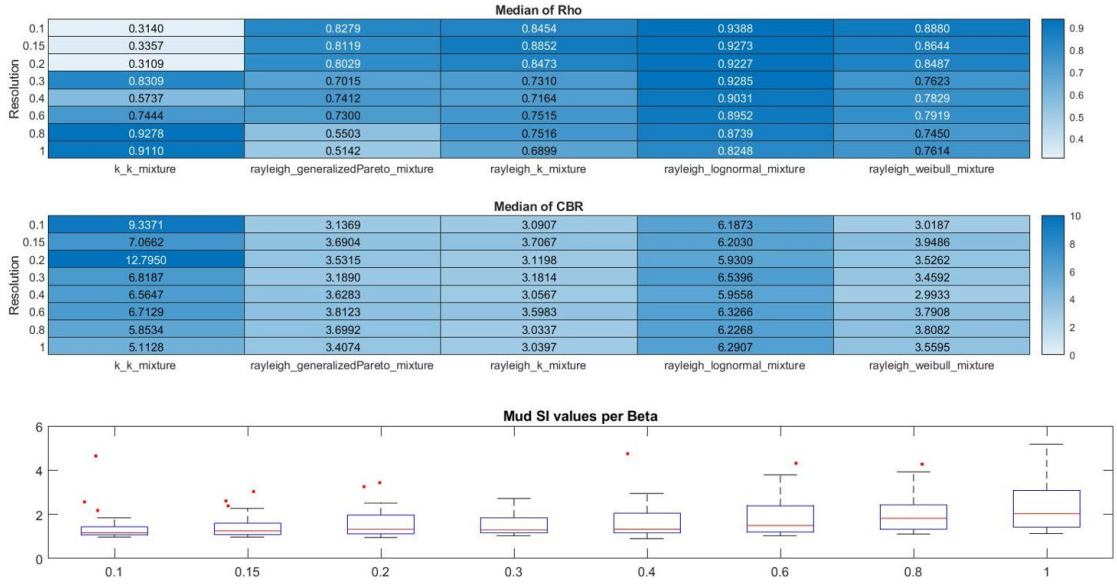

Each distribution was compared against itself for all bottom types to identify performance trends. Beginning with the K-K mixture distribution, one can see very high ρ values for Rock, Gravel, and Mud. This indicates that background pixels have a strong majority over clutter pixels for most bottom types and resolutions. This makes sense as those three bottom types have the larger scatters (making them clearer and well defined), and thus the background would dominate over the clutter. This is opposed to sand, which has much smaller and grainier scatterers, and as a result has a larger presence of clutter pixels. For the K-K mixture distribution there is a clear trend that ρ decreases with resolution reduction. This means that increased levels of resolution reduction cause the large scatters to become undefined, and more closely resemble the sand data. As such, with enough resolution reduction clutter pixels will eventually win out (although the amount of resolution reduction required for this to happen depends on bottom type, and in the case of the Rock data that point was never met). This trend is what is physically expected to occur to background and clutter pixels as resolution is reduced. The only exception for the K-K distribution is the sand bottom type, where the ρ values remain relatively constant. This makes sense for sand as the scatters are much smaller than the other bottom types, and the resolution is already grainer. Looking at the CBR data for the K-K distribution, one can

see that across the board the clutter intensity is higher than the background intensity (most CBR values fall between 5–12 for all bottom types and β values, much higher than a value of 1 which would indicate similar intensities). Additionally, there is a trend that CBR deceases with resolution reduction. However, it never approaches the point where background intensity is close to winning out. The only exception to this is the Mud CBR values, which seem to increase with resolution reduction. This was considered a potential indicator that the K-K distribution doesn't fit the mud bottom type well.

Analyzing the R-GP mixture distribution, one will see significantly different results and trends. The R-GP ρ values are very low at higher resolutions, which indicates that the clutter pixel numbers are decisively higher than the background pixel numbers. The exception to this is the sand bottom type, which has similar values to the K-K distribution. This is likely also due to the small scatterers and grainy resolution of sand. Additionally, unlike the K-K distribution, the R-GP has a trend across all bottom types where ρ increases with resolution reduction (which goes against the physical explanation). For all R-GP CBR plots the clutter pixel numbers dominate (have a value greater than one) for all β values. Looking at the R-GP CBR values, they are generally higher than the K-K distribution's CBR values (at higher resolutions). This indicates that the clutter intensity remains dominate over the background intensity for the R-GP distribution as well. The one exception to this trend is the mud distribution, which has lower R-GP CBR values at higher resolutions than K-K (although still high enough that it is clear the clutter intensity dominates over the background intensity). This might be due to how poorly K-K fits as opposed to an issue with the R-GP fit. Similar to the K-K distribution, the R-GP CBR values decrease slightly with resolution reduction. The one exception to this is also the mud bottom type, in which the CBR values remain relatively constant.

Conceptually, both the K-K and R-GP mixture distributions perform as expected with their CBR values. Both distributions have CBR values which decrease with resolution reduction (except for mud CBR values for both distributions) and have values significantly higher than 1. However, in terms of ρ, the R-GP distribution goes against the physical explanation for all bottom types. As the resolution is reduced, and the scatterers become less well defined (images become grainer), the amount of clutter pixels should increase

(and thus ρ should increase with resolution reduction like in the K-K distribution). Therefore, despite good p-value fits, the R-GP does not provide the accurate physics-based distribution this paper is searching for. The fact that the R-GP fit well despite not accurately modeling the environment is most likely because the GP is a flexible distribution that does a good job fitting the "knee" seen consistently in the PFA plots (Olson, 2019). Therefore, only the K-K mixture distribution was analyzed to develop an equation and reference table for performance of clutter and background parameters at various resolutions. While the K-K did not perform well in terms of its CBR values for the mud bottom-type, no other distribution performed well enough to be evaluated in its place (all other distributions had increasing ρ with resolution reduction like the R-GP). To better illustrate the ρ and CBR trends for the K-K distribution, Figures 22–25 display the p-values from Figures 18–21 in Box-Whisker plot format.

Figure 22. K-K Distribution Rock ρ/CBR/SI Box and Whisker Plots

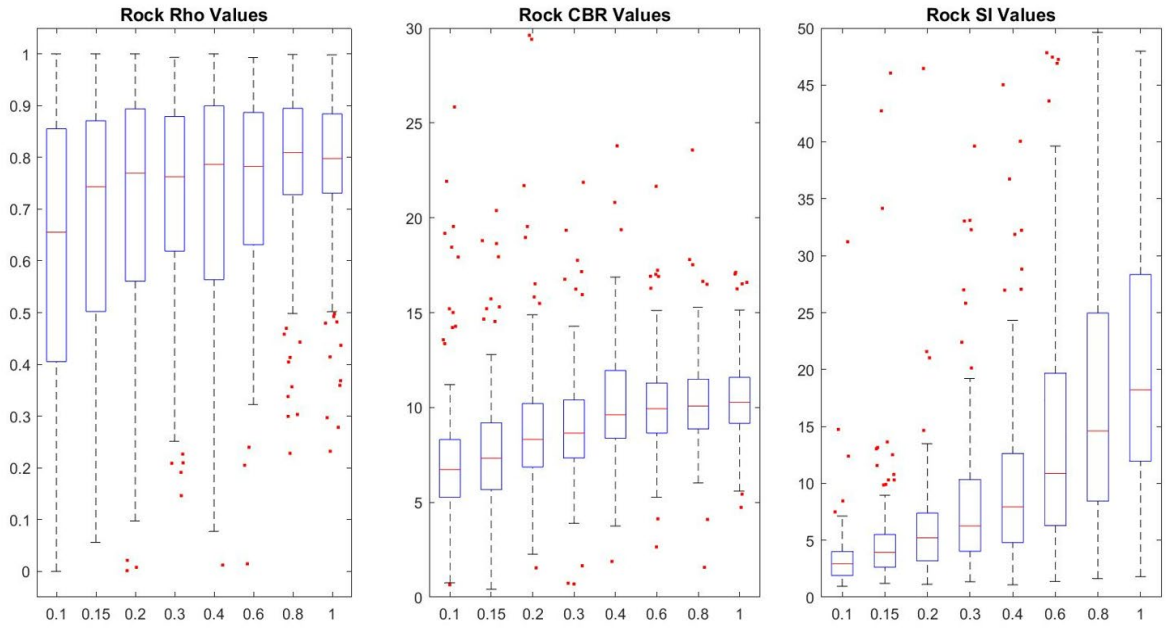

Figure 23. K-K Distribution Gravel ρ/CBR/SI Box and Whisker Plots

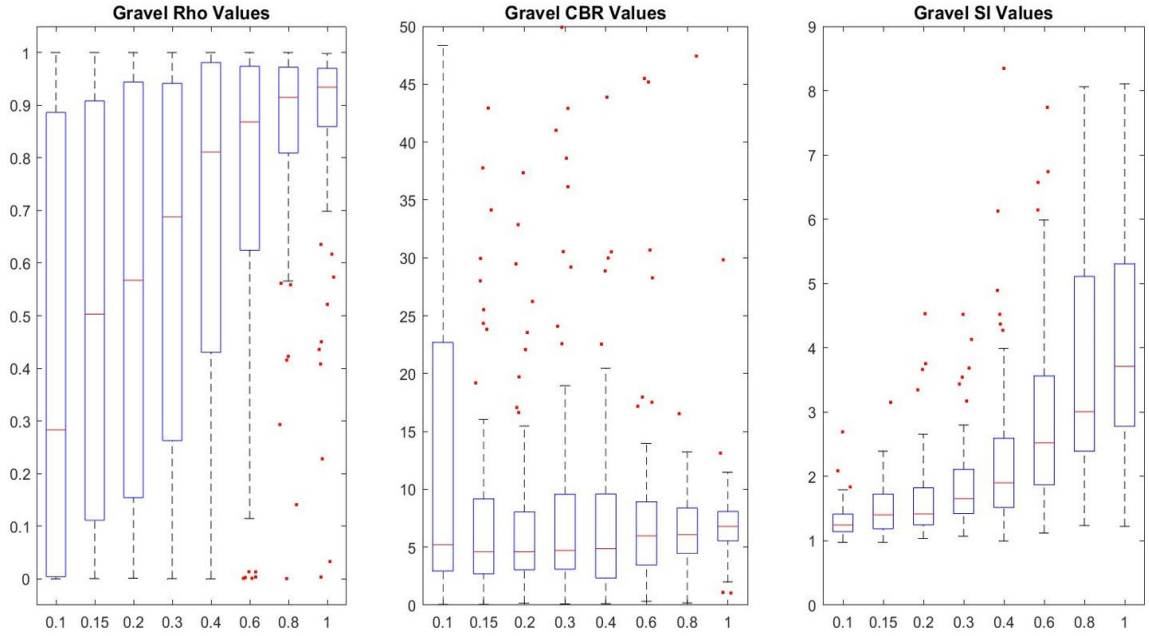

Figure 24. K-K Distribution Sand ρ/CBR/SI Box and Whisker Plots

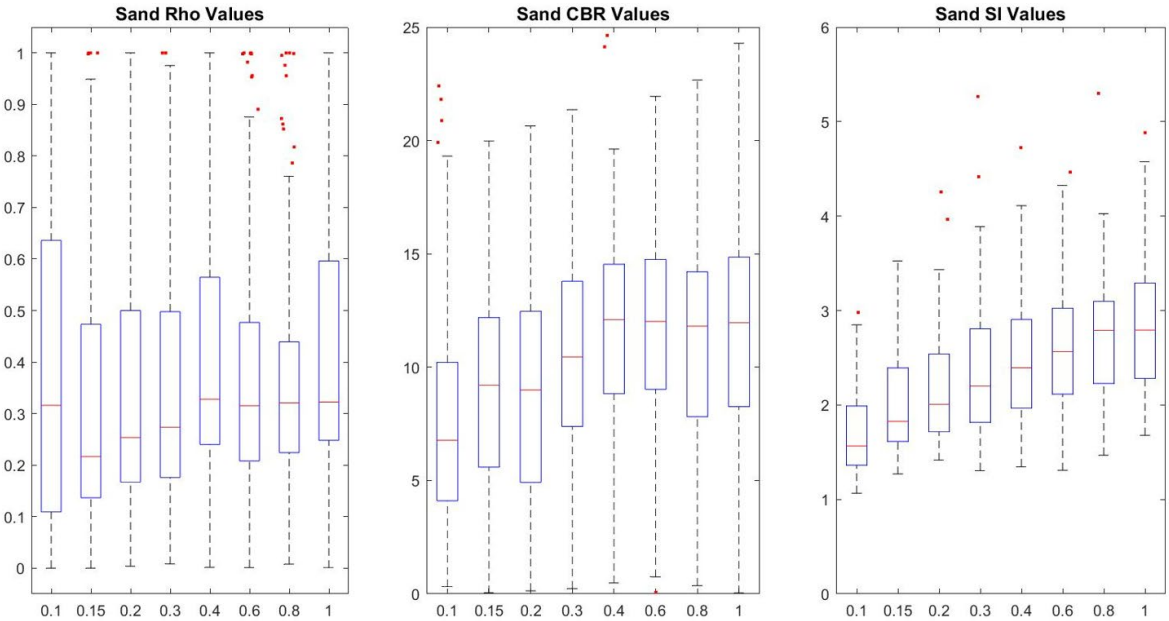

Figure 25. K-K Distribution Mud ρ/CBR/SI Box and Whisker Plots

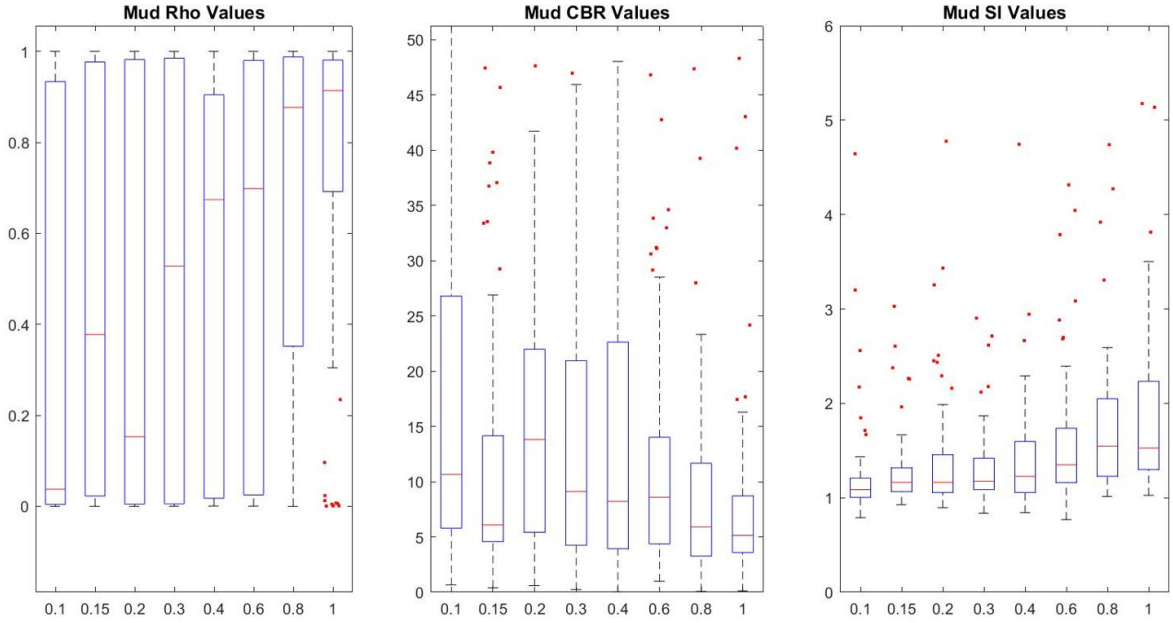

Figures 26–29 show the calculated ρ and β values from the empirical formula for the K-K distribution plotted with 95% confidence intervals (CIs). Focusing first on the CBR CI plots, the CBR values for the rock, gravel, and sand bottom types have relatively tight CIs, indicating the empirical equation can solve for the CBR values with relatively high accuracy. Another positive sign is that most of the model fits each resolution are within the 95% CIs. Gravel has a slightly worse fit than Rock and Sand, with the model fits not all falling into the CIs. However, the observed trends in the data are still captured by the model fits, the CIs are relatively tight, and the data fits are relatively close to the confidence intervals. A suggestion on how to improve Gravel bottom type fitting is included in Section VI. Focusing on the mud plots, the CIs are very large across almost all β values, and not all the model fits pass through the CIs. This makes sense since the Figures 21 and 27 show that the K-K distribution does not model the mud bottom type well. Thus, it follows that the empirical equations developed to calculate the K-K distribution's background and clutter parameters would not yield accurate results for the mud bottom type.

For the ρ CI plots, the rock plots have the tightest CI, and the median is centered closely on the model fit. However, there is a clear trend of increased CI range with resolution reduction (notably at lower β values, such as .1 and .15). This trend is also observed in the sand bottom type where the CI is tight at high β values but expands as β is reduced. The same trend seen in rock and sand bottom types is also true for the gravel bottom type. The gravel bottom type has a worse ρ fits than the other two bottom types, but still has relatively tight CI intervals and good model fits. These results indicate that background parameters can be predicted with more accuracy for higher resolution sonar systems (such as SAS) compared to lower resolution sonar systems (such as side-scan sonar at longer ranges). This suggests one can reduce high resolution SAS data to 1/2 and 1/3 its resolution and accurately predict the data sets new ρ and CBR values. However, for the mud bottom type, the ρ and CBR CIs get wider much quicker than the other bottom types, and the model does not seem to fit either parameter well. This confirms that the K-K distribution does not do a good job modeling how background and clutter parameters change with resolution reduction for the mud bottom type. The theory developed for why the model did not fit the mud data set well was that the mud data set was actually composed of two distinct subcategories of bottom types that perform quite differently. The two subcategories are homogeneous mud bottom types (no large scatterers present), and non-homogenous mud bottom types (large scatterers trapped in the mud). Looking at Figure 30, one can see how differently a snippet with a large scatterer trapped in the mud performs in relation to a snippet that is very homogenous. The non-homogenous snippet has a drastic knee that the homogeneous snippet does not. This is one example of how the mud data set might really consist of two distinct subsets. Additionally, looking at Figure 29, one can see that most of the data points have either high or low ρ values, and relatively few data points are near where the mean is. This is further proof that the K-K distribution does not fit the mud data set because of a disparity in how homogenous and non-homogenous snippets perform.

Figure 26. K-K Distribution ρ and CBR Rock CI Plots

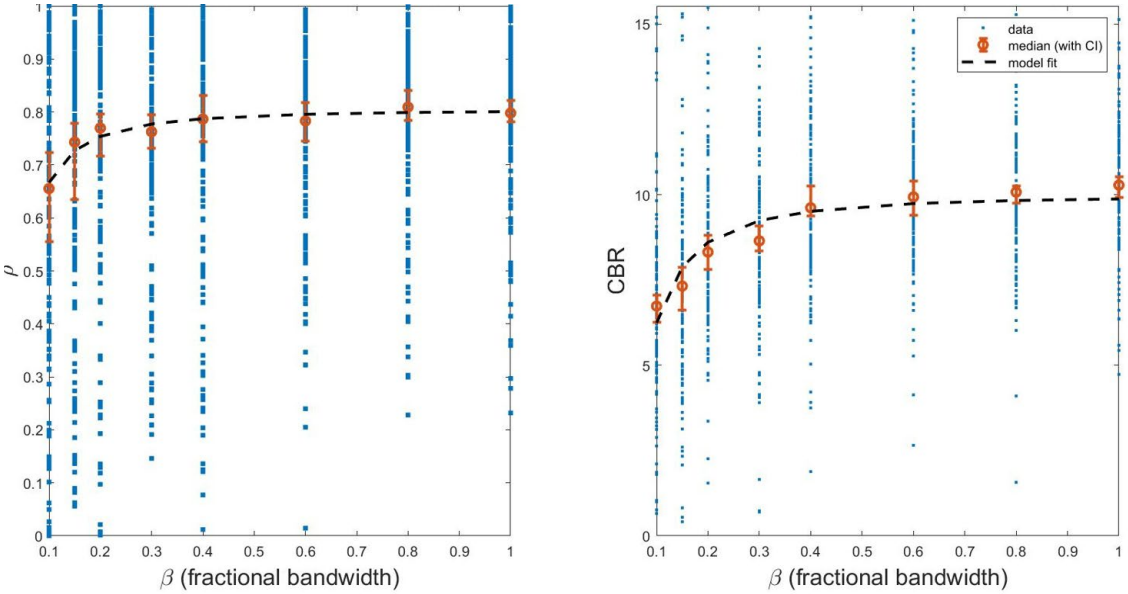

Figure 27. K-K Distribution ρ and CBR Gravel CI Plots

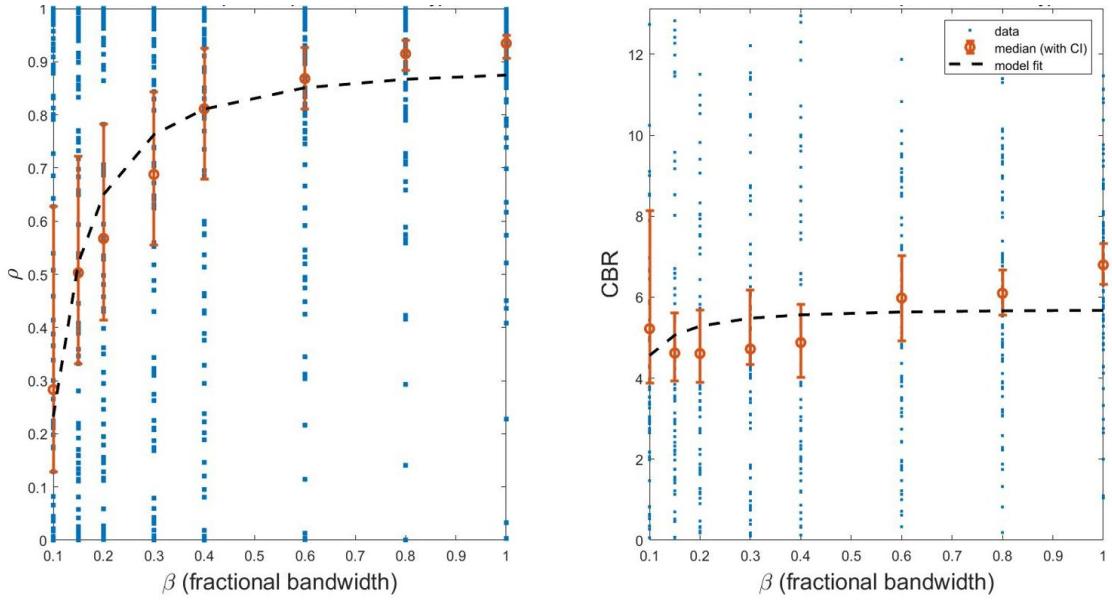

Figure 28. K-K Distribution ρ and CBR Sand CI Plots

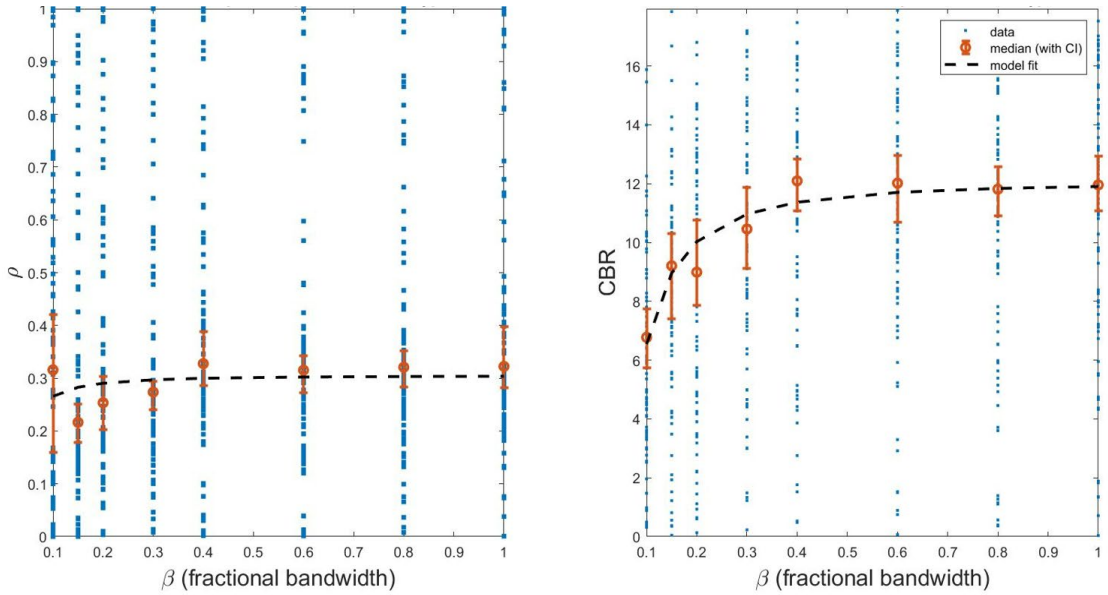

Figure 29. K-K Distribution ρ and CBR Mud CI Plots

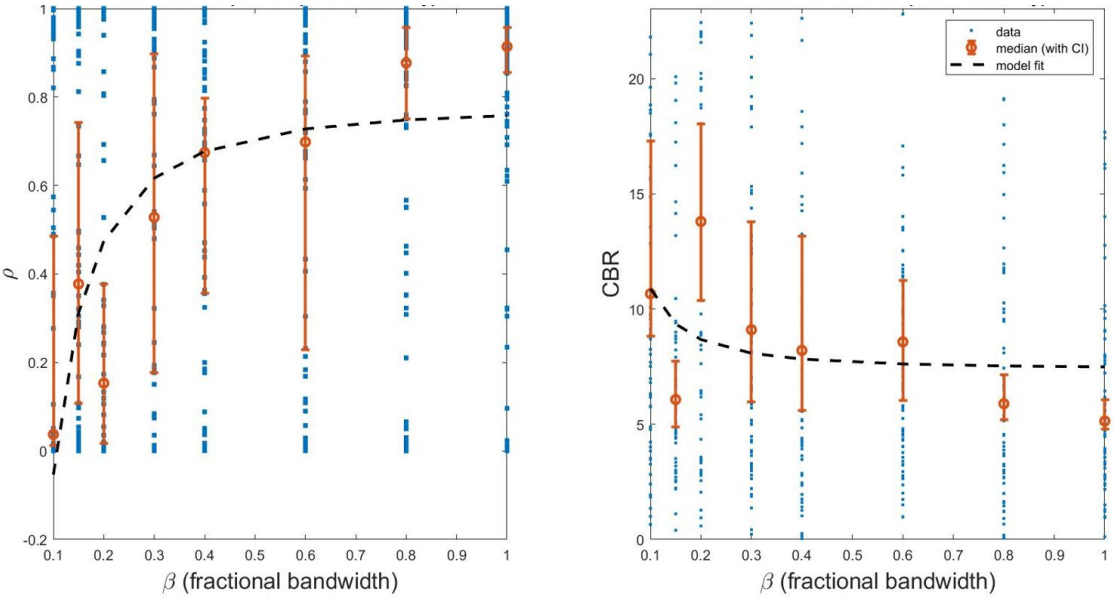

Figure 30. PFA Plots Comparing Homogenous And Non-Homogenous Mud Bottom Types

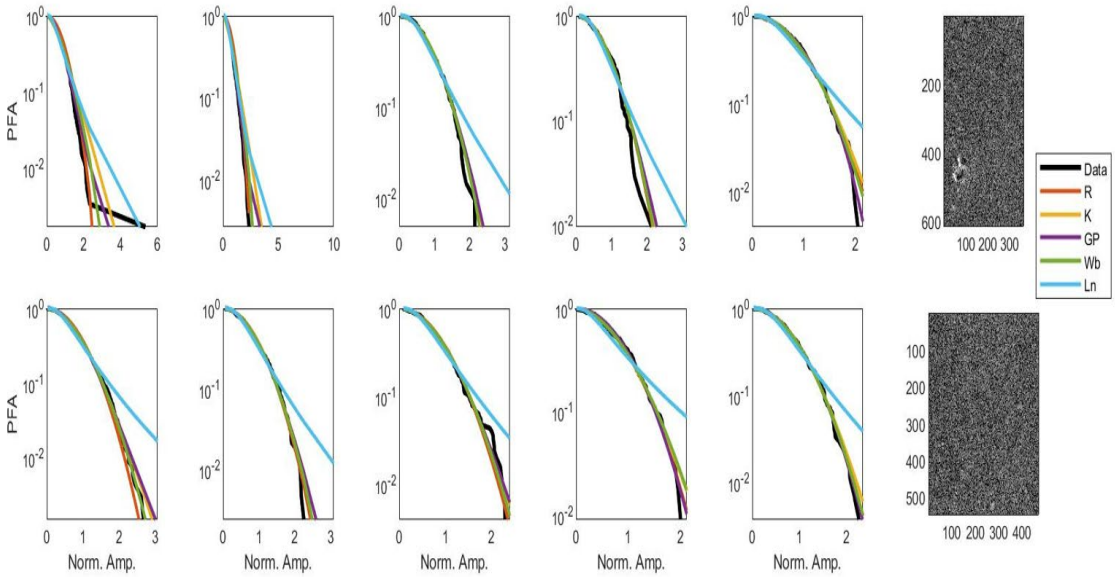

Both rows are PFA plots for β values 1, 0.8, 0.6, 0.4, and 0.2 (left to right). The top row of plots is for a mud snippet with a large object stuck in the mud (non-homogenous). The bottom row of plots is for a mud snippet that has no large objects present (homogeneous).

To test the hypothesis about homogeneous and non-homogeneous mud bottom types, two additional subcategory of mud snippets were created, each consisting of 20 new snippets. Figures 31–32 are the Mud ρ and CBR CI plots for the two new mud homogeneous and non-homogeneous data sets. Figure 31 confirms that the K-K distribution does not fit homogenous mud bottom types well. The CIs for both the ρ and CBR values are wide across all β values, and the empirical equations do not fit the environmental data well. Some of the large CI values could be attributed to less data samples (20 versus the original 82 snippets), but not enough to explain or justify the poor fits. However, Figure 31 shows that for non-homogeneous ρ values, the K-K distribution is a very good fit. The CBR CI values are a little wide, but not as bad a fit as the homogeneous bottom type, and the fit might be improved with more data points. An explanation for why the K-K distribution can fit non-homogenous but not homogeneous mud bottom types is that a mixture component model is not needed for homogeneous mud bottom types. There are not multiple types of scattering occurring, and thus single distributions like the K and GP distributions should be considered.

Figure 31. K-K Distribution Homogenous Mud ρ and CBR CI Plots

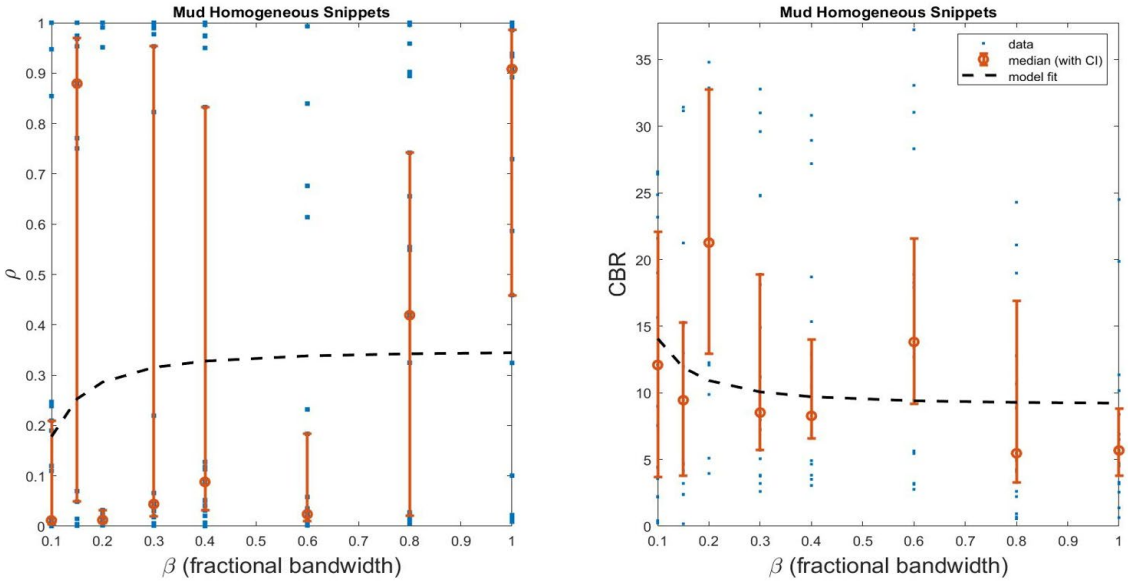

Figure 32. K-K Distribution Non-homogeneous Mud ρ and CBR CI Plots

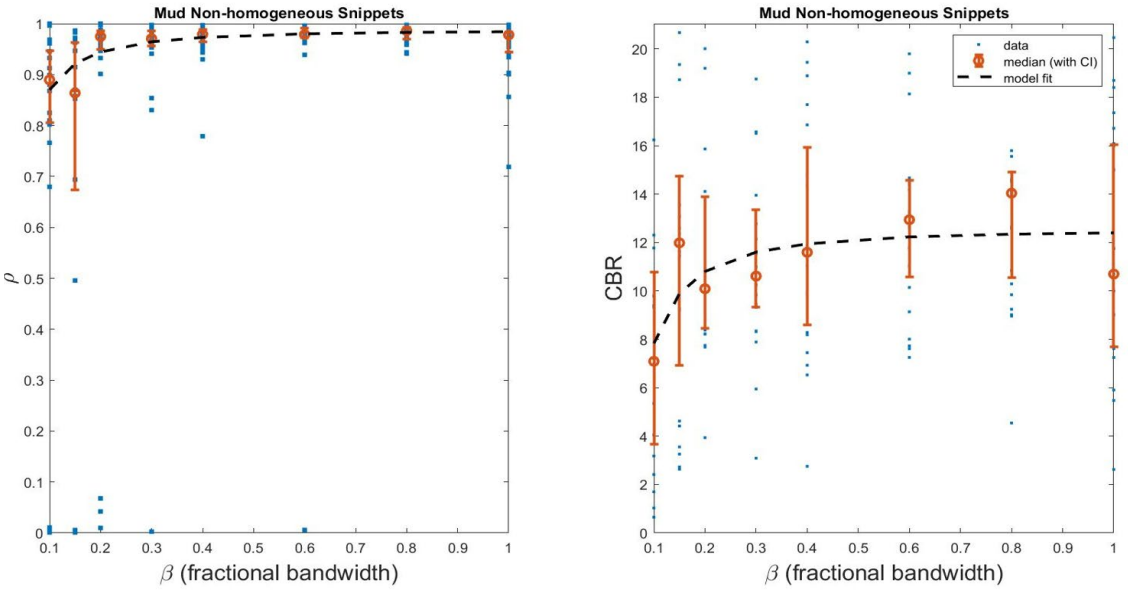

Despite the K-K distribution not performing well for the mud data set, by analyzing Figures 26–29 trends were identified which allowed for the creation of empirical equations which could be used to predict ρ and CBR values at a user's chosen resolution (β) and bottom type. The observed trends were that at β values for all bottom types, the data's

median ρ values were relatively level (therefore an empirical equation which would be nearly asymptotic for ρ at higher resolution levels was needed). For lower resolutions however, the exact opposite was true. The observed trend was a steep drop of in the median ρ values as resolution decreased (therefore an empirical equation which would reflect a steep curve for ρ at lower resolutions was needed). Similar trends for CBR were also observed across all bottom types, and therefore the empirical equation for CBR would match the format as the empirical equation for ρ.

Using the empirical equations 12 and 13, environmental constants were extrapolated from the equation since the ρ/CBR/β values were known. The environmental constants are shown in Table 3. With the empirical equations and table created, one can estimate the background and clutter parameters for a desired bottom type and frequency. This allows one to understand how sonar data will change with resolution manipulation and is the first step in connecting high resolution data with low resolution data.

Table 3. Model Parameters as a Function of β

	Rock	**Gravel**	**Sand**	**Mud**
$\boldsymbol{a_1}$	0.8006	0.8747	0.3037	0.7580
$\boldsymbol{a_2}$	0.0058	0.0279	0.0016	0.0353
$\boldsymbol{b_1}$	9.8738	5.677	11.9021	7.4889
$\boldsymbol{b_2}$	0.1577	0.0485	0.2328	-0.1475

The environmental constants used in equations 12 and 13, separated by bottom type.

THIS PAGE INTENTIONALLY LEFT BLANK

VI. SUMMARY AND CONCLUSION

This paper studied the effects of resolution manipulation during the post-processing of high-resolution data from complex seafloor environments using multi-look methods. After the SAS data was processed via smoothing, whitening, normalization, resolution reduction, and decimation, common distributions for complex seafloors were fit to the environmental data. The distributions were evaluated via KS and AU goodness of fit tests for four district bottom types: rock, gravel, sand, and mud. The K-K and R-GP mixture distributions were identified as the top performing physics-based distributions and evaluated by the background/clutter parameters of ρ, CBR, and SI. Unlike the K-K distribution, the R-GP's ρ values did not decrease with resolution reduction as a physics-based model should. Therefore, the K-K distribution was selected as the overall top performing physics-based distribution. Empirical equations for the K-K distribution were then developed to match the change of background and clutter parameters with resolution reduction for each bottom type. Using the equation, constants were developed such that given a fractional bandwidth and known bottom type, one can calculate the expected ρ and CBR for the data.

There are three major advances made by this paper. The first is the expanded amount of SAS imagery evaluated by goodness of fit parameters. Previous work that evaluated p-value distribution fits for SAS imagery used only a few snippets, while this paper examined several hundred over various bottom types and resolutions (Olson, 2019; Abraham, 2011). This paper therefore offers a more comprehensive review of distribution performance for complex seafloors and adds more credence to the theory that mixture distributions (at least 2 components or more) are needed to accurately model most complex seafloors. The second major contribution was the identification of the K-K mixture distribution as the top performing physics-based distribution for predicting the effects of resolution manipulation on background and clutter parameters. The K-K distribution did not have the top performing p-value scores across all the bottom types, notably having a poor p-value fit for rock bottom types at higher resolutions (having below a .6 p-value fit for β of 1 and 0.8). However, no distribution fit the rocky bottom type particularly well,

and the K-K distribution was in the top three physics-based distributions (top one or two other than rock) across all bottom types, and its fit improved significantly with resolution reduction. Additionally, p-values are only a metric for goodness of fit. p-values do not evaluate the dependence of distribution parameters on bottom type or resolution. That is why additional parameters, such as ρ, CBR, and SI, were included for evaluation. K-K distributions ρ and CBR trends with resolution manipulation followed what was physically expected, confirming it did a good job capturing and modeling the data's environmental features. Lastly, this paper developed empirical equations which allows one to calculate the ρ and CBR values for a user's chosen bottom-type and fractional bandwidth (resolution). This is the first step in creating a bridge toward combining sonar data created for differently configured SAS systems, and potentially combining SAS and side-scan data. The data showed that for higher resolution data, background and clutter parameters could be accurately predicted for resolution reduction up to approximately 1/2 or 1/3 the resolution. This indicates a strong possibility that SAS data from differently configured systems could be combined (or old and new SAS data), but that it would be challenging to combine SAS and side-scan sonar data (especially at longer ranges).

It should be noted that while the empirical equations performed well for the rock, sand, and gravel bottom types, it did not perform well for the mud bottom type. The theory that the mud bottom type should be subdivided into two categories, homogeneous and non-homogeneous, was tested with smaller data sets. While the non-homogeneous mud bottom types were fit reasonably well by the empirical equations, the homogeneous mud bottom types did not. This indicates that the K-K distribution is not a good fit for homogeneous mud bottom types, and that a single distribution should be considered instead.

Understanding how resolution manipulation effects sonar data's background and clutter parameters is the first step toward converting sonar data to a format and resolution compatible with another sources. For follow on work, a single component distribution could be examined to see if a homogeneous mud bottom type could be fit (most likely the K and GP distributions, as they had the best p-value fits amongst the single component distributions). Secondly, the rock, gravel, and sand bottom types could be divided into subcategories (like the mud bottom type) to further increase accuracy. This would benefit

fitting the gravel bottom type the most, as it has the weakest fit of the three (but still relatively accurate). Third, the empirical equations and the ρ/CBR constants could be tested against other data sets to further refine accuracy. Finally, the equations and constants developed in this paper could be employed in an effort to combine SAS data collected at different resolutions. The resulting operational product should then be tested for how well the data was fused and compared against a full survey conducted by one consistent sonar sensor.

THIS PAGE INTENTIONALLY LEFT BLANK

LIST OF REFERENCES

Abraham, D. A and A. P. Lyons, 2004: Reverberation envelope statistics and their dependence on sonar bandwidth and scattering patch size, *IEEE J Oceanic Eng*, **29**, 126–137, https://ieeexplore.ieee.org/document/1273568.

Abraham, D. A and A. P. Lyons, 2002: Novel physical interpretations of K-distributed reverberation, *IEEE J Oceanic Eng*, **27**, 800–813, https://www.researchgate.net/publication/3231321_Novel_physical_interpretation_of_K-distributed_reverberation.

Abraham, D. A and A. P. Lyons, 2010: Reliable methods for estimating the K-distribution shape parameter, *IEEE J Oceanic Eng*, **35**, 288–302, https://ieeexplore.ieee.org/document/5427057.

Abraham, D. A, J. M. Gelb, and A. W. Oldag, 2011: background and clutter mixture distributions for active sonar statistics, *IEEE J Oceanic Eng*, **36**, 231–247, https://www.semanticscholar.org/paper/Background-and-Clutter-Mixture-Distributions-for-Abraham-Gelb/3abed4183735e2ca3effecd092bfec6feec08a54.

Abramowitz, M. and I.A. Stegun, 1970: *Gamma Function and Related Functions: Handbook of Mathematical Functions*. Dover Publications, 253–294.

Abramowitz, M. and I.A. Stegun, 1970: *Probability Functions: Handbook of Mathematical Functions*. Dover Publications, 925–96.

Becker, K. M., 2004: Effect of various surface-height-distribution properties on acoustic backscattering statistics, *IEEE J Oceanic Eng*, **29**, 246–259, https://ieeexplore.ieee.org/document/1315716.

Bellettini, A. and M. Pinto, 2009: Design and experimental results of a 300-kHz synthetic aperture sonar optimized for shallow-water operations, *IEEE J Oceanic Eng*, **34**, 285–293, https://ieeexplore.ieee.org/document/4674519.

Chotiros, N. P., 2010: Non-Rayleigh distributions in underwater acoustic reverberation in a patchy environment, *IEEE J Oceanic Eng*, **35**, 236–241, https://ieeexplore.ieee.org/document/5392966.

Chotiros, N. P., H. Boehme, T. G. Goldsberry, S. P. Pitt, A. Lamb, A. L. Garcia, and R. A. Altenburg, 1985: Acoustic backscattering at low grazing angles from the ocean bottom. Part II. Statistical characteristics of bottom backscatter at a shallow water site, *J. Acoust. Soc. Am*, **77**, 975–982, https://asa.scitation.org/doi/10.1121/1.392065.

Davison, A. C., and D. V. Hinkley, 1997: *Bootstrap Methods and Their Applications*. Cambridge University Press, 594 pp.

Hansen, R. E., H. J. Callow, T. O. Sæbø, and S. A. V. Synnes, 2011: Challenges in seafloor imaging and mapping with synthetic aperture sonar, *IEEE Trans. Geosci. Remote Sensing*, **49**, 3677–3687, https://ieeexplore.ieee.org/document/5937049.

Hjelmervik, K. T., 2010: Predicting sonar false alarm rate inflation using acoustic modeling and a high-resolution terrain model, *IEEE J Oceanic Eng*, **35**, 278–287, https://ieeexplore.ieee.org/document/5433232.

Hydro International, 2019: Swire seabed orders HUGIN autonomous underwater vehicle. Accessed 19 May 2022, https://www.hydro-international.com/content/news/swire-seabed-orders-hugin-autonomous-underwater-vehicle.

Jackson, D.R. and M. D. Richardson, 2007: *Seafloor Roughness. High-Frequency Seafloor Acoustics*, Spring Science+Business Media, 171–198.

Johnson, S. F., 2009: Synthetic aperture sonar image statistics, The Pennsylvania State University, 150 pp.

Lyons, A. P. and D. A. Abraham, 1999: Statistical characterization of high-frequency shallow-water seafloor backscatter, *J. Acoust. Soc. Am.*, **106**, 1307–1315, https://asa.scitation.org/doi/10.1121/1.428034.

McDaniel, S. T., 1990: Seafloor reverberation fluctuations, *J. Acoust. Soc. Am.*, **88**, 1530–1535, https://asa.scitation.org/doi/10.1121/1.400310.

Olson, D. R., D. A. Abraham, A. P. Lyons, and T. O. Sæbø. 2019: Scattering statistics of rock outcrops: Model-data comparisons and Bayesian inference using mixture Distributions, *Acoust. Soc. Am.*, **145**, 761–774, https://asa.scitation.org/doi/10.1121/1.5089892.

Sæbø, T. O., H. J. Callow, R. E. Hansen, B. Langli, and E. O. Hammerstad, 2007: Bathymetric capabilities of the HISAS interferometric synthetic aperture Sonar, *OCEANS 2007 MTS/IEEE*, https://ieeexplore.ieee.org/document/4449357.

Strutt, J. W., 1919: On the problem of random variables, and of random flights in one, two, or three dimensions, *The London, Edinburgh, and Dublin Philosophical Magazine and Journal of Science*, **6**, 331–347.

Williams, D. P., 2018: The Mondrian detection algorithm for sonar imagery, *IEEE Transactions on Geoscience and Remote Sensing*, **56**, 1091–1102, https://ieeexplore.ieee.org/document/8070463.

INITIAL DISTRIBUTION LIST

1. Defense Technical Information Center
   Ft. Belvoir, Virginia

2. Dudley Knox Library
   Naval Postgraduate School
   Monterey, California